論文 / 著書情報
Article / Book Information

題目(和文)	
Title(English)	Elucidating transformation products and its formation mechanism during advanced oxidation processes of organic compounds by in silico and experimental approaches
著者(和文)	DWINANDHA Dhimas
Author(English)	Dhimas Dwinandha
出典(和文)	学位:博士(学術), 学位授与機関:東京工業大学, 報告番号:甲第12598号, 授与年月日:2023年9月22日, 学位の種別:課程博士, 審査員:藤井 学,鼎 信次郎,吉村 千洋,内海 信幸,中村 隆志
Citation(English)	Degree:Doctor (Academic), Conferring organization: Tokyo Institute of Technology, Report number:甲第12598号, Conferred date:2023/9/22, Degree Type:Course doctor, Examiner:,,,,
学位種別(和文)	博士論文
Category(English)	Doctoral Thesis
種別(和文)	要約
Type(English)	Outline

Elucidating transformation products and its formation mechanism during advanced oxidation processes of organic compounds by in silico and experimental approaches

By

Dhimas DWINANDHA

Supervised by

Associate Professor Manabu FUJII

A dissertation submitted to the Department of Civil and Environmental Engineering, School of Environment and Society, Tokyo Institute of Technology, in partial fulfilment of the requirements for the degree of Doctor of Philosophy

July 2023

ABSTRACT

Advanced oxidation process (AOP) treatments, especially OH•-based process, have been proven as an effective method to eliminate organics in the water while also being easy to implement at a low cost. However, recent studies suggested AOP treatments may not remove the organics completely—the organics are merely transformed into more toxic transformation products (TP). Thus, assessment of TPs from AOPs treatment of organic compounds are significantly needed, particularly assessment of transformation mechanism and resulting products. In this thesis, in silico and experimental methods were employed to give information about: (i) reactivity of organic compounds in OH•-based process; (ii) transformation mechanism from parent compounds to their TPs and its key reaction pathways. In the first part of the research, a theoretical investigation using quantum chemical calculations was conducted to understand the OH•-mediated oxidation mechanism of phenol. Different levels of theory were compared, and the most accurate predictions were obtained using the M06-2X level of theory. The study successfully predicted the reaction sites and rate constants for the formation of transformation products hydroquinone and catechol and demonstrates the potential of quantum chemical calculations for investigating the formation mechanisms of TPs in AOPs for organic compound removal in water environments. The second part of the research utilized isotopically labelled FT-ICR-MS, combined with machine learning techniques and paired mass distance (PMD) network analysis, to explore the reactivity and transformation of natural organic matter (NOM) during UV irradiation. The reactivity of different molecular formulas and structural categories was examined, with CHOS-formulas exhibiting the highest reactivity. The interpretable machine learning algorithm identified key features governing the reactivity, such as molecular weight, DBE-O, NOSC, and the presence of heteroatoms (N and S). Similarly, the last part investigates lignin reactivity and transformations as a model compound for natural organic matter during UV photolysis using FT-ICR-MS analysis, interpretable machine learning, and PMD analyses. The study reveals aliphatic hydroxyl groups as the most reactive functional groups in the initial stage of UV exposure, while phenolic hydroxyl groups were the most reactive in the later stage. Furthermore, hydroxylation and ketonization/quinone production were found as the primary transformation processes during the initial irradiation, while dealkylation and deformylation reactions were seen subsequently, indicating aromatic ring oxidation and cleavage. The findings contribute to understanding natural organic matter degradation in photo-oxidation systems. Overall, the outcomes of this study have significant implications for water treatment strategies, enabling the design of more efficient Advanced Oxidation Processes (AOPs) and providing insights into the dynamics of organic compound degradation in water systems. Furthermore, the findings contribute to the assessment of environmental transformation products, assisting in the mitigation of potential risks associated with the production of toxic substances in water.

ACKNOWLEDGEMENT

Firstly, I would like to express my deep gratefulness to my supervisor, Associate Professor Manabu Fujii, who kindly provides me with his guidance, advice, and mental support to conduct this study and my life in Japan in general, as well. His vast knowledge and wisdom helped me carrying out this study and writing this thesis, which I really appreciate. I am also thankful the reviewers who dedicated their valuable criticisms to improve my research.

I would like to acknowledge the Japanese Ministry of Education, Culture, Sports, Science, and Technology (MEXT) for giving me the scholarship to have an opportunity to pursue my study in Tokyo Institute of Technology. I am also extremely grateful to have all my graduated and current lab members for their assistance and helpfulness. To my secretaries, Takahashi-san your sincere care and kindness are really appreciated.

Finally, I cannot express enough gratitude to my family in Indonesia, for whom I have the greatest strength to continue my study and live in Japan. My acknowledgement also goes to my close friends, both in Indonesia and Japan, for continuously providing me consolation, encouragement, laughter, and even just ears that are ready to listen throughout these years.

TABLE OF CONTENT

CHAPTER I General Introduction

I.1. Transformation products from advanced oxidation process of organic pollutants in aquatic environment

I.1.1. Organic pollutants and their presence in aquatic environment

Organic pollutants are a significant concern in the aquatic environment due to their adverse effects on both aquatic organisms and human health[1–3]. Their presence in aquatic ecosystems can arise from various sources, such as industrial and agricultural activities, urban runoff, domestic wastewater discharge, and microbial decaying process[3]. Many of these organic pollutants are refractory and once introduced into water bodies, various organic pollutants can persist for extended periods and undergo bioaccumulation through the food chain, leading to potential biomagnification. Consequently, the accumulation of these pollutants in aquatic organisms can result in physiological, reproductive, and developmental abnormalities, as well as impairments to the overall ecological balance of the aquatic ecosystem[3]. For example, accumulated pesticides (organophosphate, N-methylcarbamates and pyrethroids) in human body pose seriously threat to thyroid function[4]. Thus, research about the removal technology for such compounds has always been a huge topic in environmental studies to eliminate the risk of organic pollutant exposure to human and environment.

I.1.2. Removal technology and transformations of organic pollutants in water treatment

Water and wastewater treatment plant is a crucial point that act as a protection barrier from organic pollutants exposure to human and environment. In conventional treatment plant for example, various treatment methods are implemented: activated sludge, coagulation-flocculation-sedimentation, rapid sand filtration, and chlorination, to name a few. Generally, it targets the biodegradable and colloidal organics. However, conventional treatment plants are not designed to remove organic micropollutants (OMP) such as pharmaceuticals, pesticides, and personal care products thus have poor treatment efficiency[5,6]. Exacerbated by the global use of those chemicals, it is not surprising they are frequently detected in effluents, surface waters and tap water[7].

In the past few years, advanced oxidation processes (AOPs) have gained a lot of interests due to their potential in degradation of organic pollutants For example ozone[8], UV[9], Fenton reaction[10], electrochemical reaction[11], and photocatalysis[12] are employed to remove organic micropollutants (OMPs) mainly by radical oxidation. Most of AOPs are specifically designed to produce hydroxyl radicals (·OH) due to its strong oxidative nature owing to its high oxidation potential of 2.8 V[13], allowing it to react with a large variety of OMP in the

water[14]. Hydroxyl radicals can oxidize OMPs and convert them into low molecular-weight compounds[13,15] with the rate constants ranging from 10^8 to 10^{10} M/s[16]. The utilization of AOPs for the removal of various OMPs, such as acetaminophen, atenolol, caffeine, carbamazepine, diclofenac, ibuprofen, and trimethoprim, has been discussed in the literature for laboratory-scale and pilot-scale treatments[17–21].

Table I-1 Detected TPs in WWTP effluents in some countries

Parent Compound	WWTP location	Max concentration (ng/L)	Reference
VFX	Canada	1454	[22]
O-DMV	Canada	3131	[22]
ODN	Kallby	2510	[23]
CBZ	Canada	1325	[24]
MTPA	Spain	2116	[25]
CTP	USA	280	[26]
DCPG	USA	194	[26]
AMPH	Germany	190	[27]
DCF	Montcada	642	[28]
LAS	Germany	9205	[29]

However, in most cases, organic pollutants including OMPs are not completely mineralized by AOPs but are partially oxidized into transformation products (TPs). There have been many reports of detected TPs in the treated water, as shown in Table I-1. The formation of TP in AOP are resulted from three major reactions of $^{\bullet}OH$ with organics: (1) hydrogen abstraction, (2) electrophilic addition or hydroxylation, and (3) electron transfer[30].

$$^{\bullet}OH + SH \rightarrow {}^{\bullet}S + H_2O \quad (1)$$
$$^{\bullet}OH + FX \rightarrow {}^{\bullet}HOFX \quad (2)$$
$$^{\bullet}OH + SX \rightarrow SX^{+} + HO^{-} \quad (3)$$

The predominant type of reaction of $^{\bullet}OH$ with organic compounds is hydrogen abstraction, followed by hydroxylation, and electron transfer. The product of reaction (1) is carbon-centred radicals ($^{\bullet}S$), which can further react with dissolved oxygen to start subsequent oxidation reactions. Meanwhile, electron transfer to the $^{\bullet}OH$ results in reduction of $^{\bullet}OH$ to hydroxide anions (HO^{-}), and mainly occurs in inorganic compounds[31]. Hydroxylation, which mainly occurs on olefins or aromatic rings of pollutants, produce hydroxylated by-products ($^{\bullet}HOFX$). Then it will be further oxidized via kentonization and

carboxylation to generate the final products aldehydes and aliphatic acids[32]. Aside from those reactions, the TPs generated from dealkylation on C-N or C-O bonds, decarboxylation and deamination on alkyl chains or aromatic rings during UV/H_2O_2 and UV photocatalysis of contaminants have been reported as well[33–36]. It should be emphasized, that the reactions described above are only a fraction of all reactions during pollutants degradation. Other reactive species (such as O_2^-) and intermediates may develop in the reaction system as the process progresses, which makes the mechanism of the tested pollutant degradation more complicated. Process parameters, such as the presence of oxygen and organic materials, are also significant[18,37–39].

I.1.3. Delayed awareness of the presence of AOP-TPs

Even though it has been detected all over the world, the presence of AOP-TP in the AOP research was tend to be overlooked. Figure I-1 displays the number of research articles published in the past 15 years (2007-2023) in selected academic journals in the field of water environment (Chemosphere [Elsevier], Environmental Science and Technology [American Chemical Society], Journal of Hazardous Materials [Elsevier], Science of the Total Environment [Elsevier], and Water Research [Elsevier]) using keywords “transformation product” and “advanced oxidation process”. Even from 2007-2011, the number of research related to AOP is already significant in contrast to TP-AOP. TP-AOP started to gain more interest in the research community in the year of 2016. However, the number of publications of AOP-TP is not as progressive as the AOP research itself, despite the limited knowledge of TP and global implementation of AOP for water treatment.

Analytical or experimental approach for detecting the TP can be attributed as a major factor of such delay of awareness. Unlike OMP which can be detected straightforward, for example using liquid chromatography coupled with mass spectrometry (LC-MS), it is not the case for TP itself. Since the absence of standards for most TP, targeted measurement is mostly not accessible. On the other hand, non-target exploration could be an option where high resolution mass spectrometry (HRMS) is available. Even so, both approaches still require tremendous amount of manpower, time, and cost to assess the TP.

I.1.4. Environmental concerns of organic transformation products

The concerns regarding TP in the environment rise from even at low concentrations, TPs can harm the ecosystems, endanger the health of people and other living things, and interfere with the efficient operation of AOPs[40–42]. Generally, harmful TPs can be classified

into toxic TPs, assimilable TPs, and sensory-unpleasant TPs by their potential risk[43]. Toxic TPs are harmful molecules due to its effect to a wide range of organisms such as inhibiting the activity of luminescent bacteria, being cytotoxic or genotoxic to mammalian cell, and being eco-toxic to microalgae, daphnia manga, and fish[44–46]. On the other hand, assimilable TPs are bioavailable molecules that can support the growth of heterotrophic microorganism and promotes the accumulation of biomass, which may decrease the water quality and produce sensory-unpleasant products[47–49]. Moreover, sensory-unpleasant TPs may reduce the organoleptic quality from unpleasant tastes and odors[50].

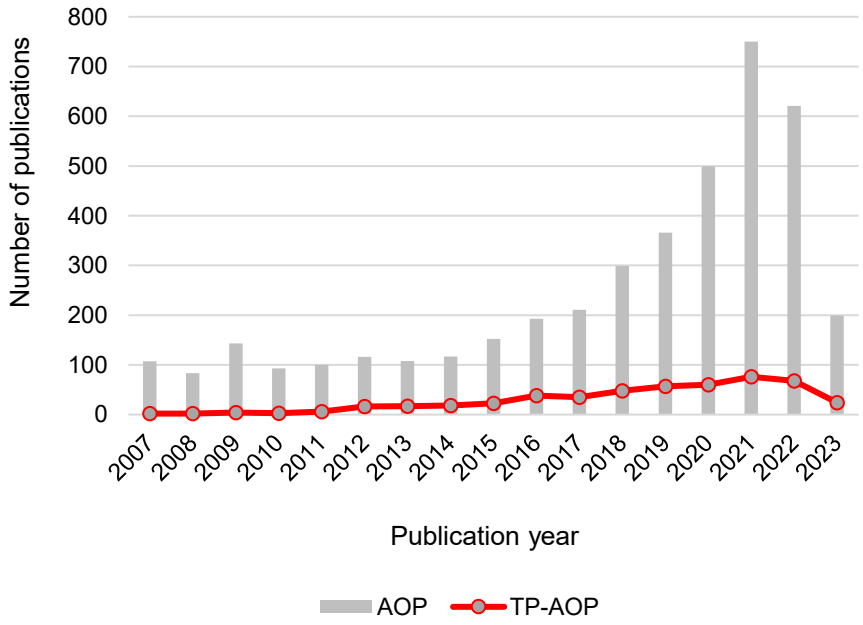

Figure I.1 Number of publications obtained with keywords “transformation product” and “advanced oxidation process” (red line) and only “advanced oxidation process” (grey bar).

It is still a challenging aspect to experimentally measure the toxicity of TPs due to various reasons. However, some studies have been reported the possibility of relationship between changes in toxicity and the corresponding molecular changes during AOP. For example, dealkylation on C-N and C-O bonds, may lead to produce toxic TPs as observed for venlafaxine[51], methotrexate[36], tramadol[52], and atrazine[53]. In addition other reactions which produced toxic TPs as well were observed in hydroxylation of atrazine[53], gabapentin[54], and diuron[55]; deamination of carbamazepine[56] and methotrexate[36], and decarboxylation of ibuprofen[57]. However, few studies have quantitatively reported the toxicity of specific TPs. One study found carboxylic acids were moderately toxic to luminescent bacteria while

ketones and aldehydes were reported to be more toxic than numerous parent micropollutants when exposed to luminescent bacteria, microalgae, and daphnia magna[58].

I.1.5. Reliability of current assessment strategies

An alternative approach to assess the toxicological status of an AOP is to evaluate the reaction mechanism of OMP with radicals produced during the process. This ideally includes qualitative and quantitative information on the identity of transformation products. Several techniques are commonly implemented for quantitative measurement: from bulk analysis (e.g. using TOC, UV spectra, optical properties), targeted analysis (e.g. using GC-MS, LC-MS, NMR), and a combined analysis from bulk and targeted with statistical for even more insight and prediction of future cases. Several example studies have reported for acesulfame[59], sulfapyridine[60], ofloxacin[61], diclofenac[62], nitenpyram[63] carbamazepine[64], ciprofloxacin[65]. However, by considering the amount of OMP presents in the environment, relative complexity of samples generated after AOP, and cost/unavailability of standard materials, the extensive quantitative measurements are not the easiest option available for assessing TP[66]. On contrast, qualitative non-targeted analysis may serve as a more applicable option for TP identification.

The backbone of qualitative non-targeted analysis is high resolution mass spectrometry (HRMS). While the targeted strategy typically requires the use of accurate standards and specifically targets the precursor or/and product ions of the potential transformation products identified prior to the analysis[67–70], the non-targeted strategy solely depends on HRMS techniques' capacity to measure molecular masses with extremely high precision[67,69–71]. Furthermore, the high-resolution data of masses obtained after analysis, which might include the exact masses of precursor (MS mode) and product (MS/MS and MS^n mode) ions, are utilized to determine the elemental composition and eventually correlate with potential structures and transformations by various means, for example by matching with a database or manually analysing the molecular formula, elemental composition, and accurate masses of the precursor and product ions[70,72,73]. In this sense, a series of post-HRMS analysis are crucial, for example using bio/cheminformatics or machine learning to assist the understanding of the obtained molecular information from HRMS. Yet, to this date the examples are still limited.

Despite the potential, several challenges, however, need to be addressed to improve the reliability of existing MS-based methodologies. Menacherry, et al.[66] describe the challenging aspects of MS for TP assessment: (1) structural elucidation still could not be

obtained in high confidence unless it is coupled with other separation techniques such as UPLC, however, achieving this information demands extensive resources (manpower, cost, and time), even more because the lack of authentic standards for TP itself; (2) the ionization component, which is necessary to ensure this crucial process of a mixture of numerous numbers of totally unknown molecules, may be too complicated.; and (3) the characterization of high-resolution mass spectra to elemental compositions and potential structures using existing tools, such as online databases and other software-based compound suggestion tools, is still very primitive.

Leading from the above issues, interests on computational or in silico-based assessment is currently growing. Several tools had been attempted to analyse TP formation and reactivity, for example using quantum chemical calculation (QCC). QCC is a theoretical approach based on the Schrödinger equation to analyse the atomic interaction in the compound molecule, including electronic structure, molecular energies, and transition state, which then are translated as reactive sites and reaction rate constants. In this case, previous studies have successfully implemented QCC for bisphenol A[74], para-substituted phenolic compounds[75], acetone[76], and ibuprofen[77]. Not only it gave a deeper understanding about the reactivity and transformation mechanisms, QCC also significantly reduces cost of analysis and duration. Nevertheless, the existence of QCC in those studies were not yet serve as a substitute of experimental approach, but rather complimentary to validate the experimental results or to gain more insight about the reaction mechanism. A full investigation of TP using only QCC is certainly possible but less studied, therefore it is needed to assess the feasibility of substitution from experimental to QCC.

Figure I-2 summarizes the area of well- and less-studied research in terms of sample complexity (simple/pure to complex/mixture) and methodological approach (experimental to in silico).

I.2. Objectives and thesis outline

The overall objective of this study based on the given background and research gap is to assess the transformation products during AOP treatment of organic compounds, specifically in OH radical-mediated process using in silico and/or experimental approach. The assessments will include the reactivity of the parent compounds, factors influencing the reactivity of the parent compounds; and formation mechanisms of the transformation products. Specifically, the exact objectives are as follows:

a) investigating the feasibility of theoretical approach as an alternative for assessing the transformation products of organic compounds during AOP;

b) combining experimental and in silico as post-experimental analysis to investigate the transformations of naturally-occurring organic matter during AOP.

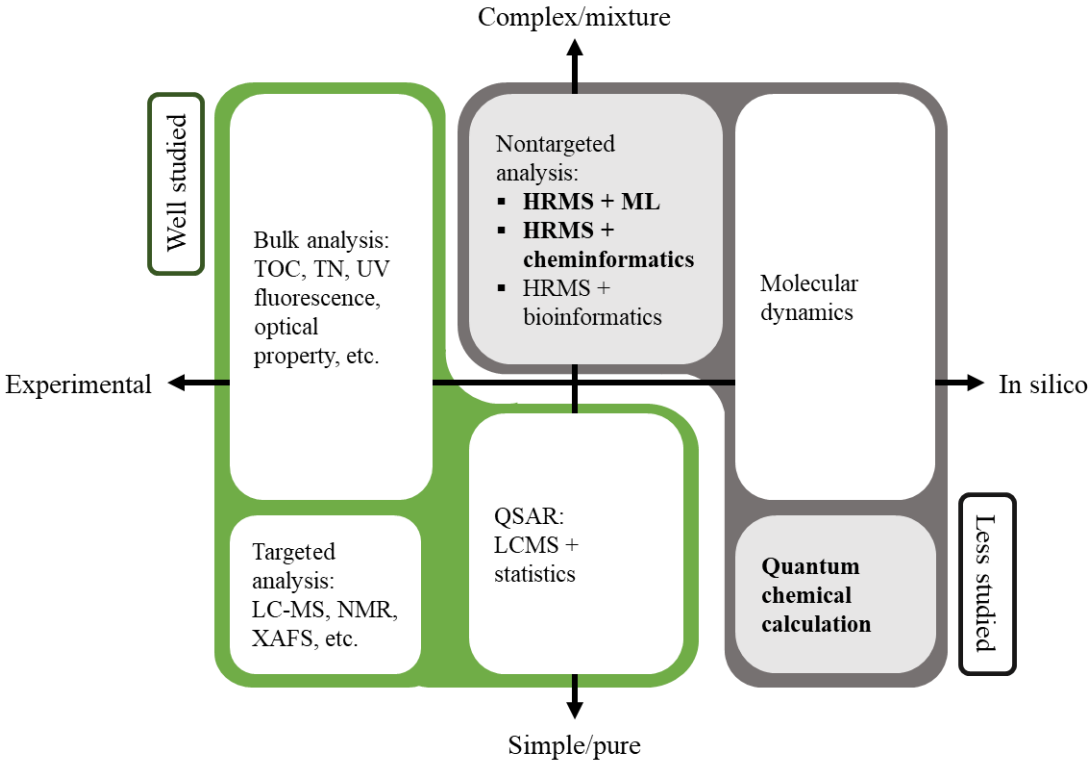

Figure I.2 Map of current assessment studies on TP highlighting the area of well- and less-studied research field

Overall, understanding the reaction characteristics of transformation products formation would contribute to the scientific knowledge of AOP reaction with organic pollutants enabling the design of more efficient AOPs and providing insights into the dynamics of organic compound degradation in water systems. For example, the reactivity of parent compounds will affect the relevant series of treatment to avoid the formation of susceptible toxic TPs. Furthermore, the reactor design can be influenced by the rate of TP formation, which is reflected by the reaction rate constant. Moreover, the assessment of TP formation will provide a new perspective about the environmental risk assessment of AOP technologies for a better implementation.

The thesis is structured as described below:

1. Chapter 1. Introduction

   This chapter discusses the background, research gap, and objectives of the thesis.

2. Chapter 2. Theoretical investigation of reaction mechanism for OH radical-mediated phenol oxidation using quantum chemical calculation

   This chapter provides the feasibility study of full theoretical approach for TP-AOP assessment using quantum chemical calculations and phenol as model compound.

3. Chapter 3. Interpretable machine learning and reactomics assisted isotopically labelled FT-ICR-MS for exploring reactivity and transformation of natural organic matter during UV photolysis

   This chapter combines interpretable machine learning and reactomics (as in silico method) and isotopically labelled FT-ICR-MS (as experimental method) to elucidate natural organic matter transformations in UV process.

4. Chapter 4. Deciphering lignin reactivity and transformations in UV photolysis studied by FT-ICR-MS and interpretable machine learning

   This chapter focuses on the reactivity and transformations of lignin as model compounds and precursor of natural organic matter during UV treatment using interpretable machine learning and reactomics combined with FT-ICR-MS.

5. Chapter 5. Conclusions and recommendations

   This chapter outlines the key findings in this study and provides recommendation for future studies.

CHAPTER II Theoretical Investigation of Reaction Mechanism for OH radical-mediated Phenol Oxidation using Quantum Chemical Calculation

Related publication:

Dwinandha, D., Zhang, B., Fujii, M. 2022. Prediction of reaction mechanism for OH radical-mediated phenol oxidation using quantum chemical calculation. Chemosphere 291, 132763. https://doi.org/10.1016/j.chemosphere.2021.132763

II.1. Introduction

Organic micropollutants (OMPs) are a diverse group of organic compounds including pesticides, pharmaceuticals, personal care products, steroids, polycyclic aromatic hydrocarbons, and other industrial organic compounds[2]. OMPs have been detected in wastewater and natural water bodies all over the world, which possesses potential hazard to human health and ecosystems due to biological accumulation and chronic toxicity[78–81]. Especially, OMPs are hard to be removed during conventional water and wastewater treatment processes. Thus, there are increasing researches to develop novel wastewater treatment techniques for removal of OMPs, such as the advanced oxidation processes (AOPs). Specifically, ozone[8], UV[9], Fenton reaction[10], electrochemical reaction[11], and photocatalysis[12] were employed to remove OMPs during AOPs. The reactive oxygen species, such as hydroxyl radicals (OH•) are commonly generated, resulting in the oxidative degradation of OMPs[82]. However, the reaction mechanism of OH•-mediated oxidation of OMPs is still amphibology in AOPs. Specially, the formation of transformation products (TPs) during the oxidation of OMPs is undefined due to the complicated and transient reactions during AOPs[14].

The occurrence of TPs in the water environment has triggered emerging concern regarding their effects on human health and environment[83]. For example, it is now well recognized that phenol TPs generated from AOPs (e.g., hydroquinone and p-benzoquinone) have a higher toxicity than phenol itself[84]. Furthermore, the other OMPs such as atrazine, caffeine, diclofenac, carbamazepine, and triclosan have been reported to generate TPs with higher toxicity than their parent compounds[85]. While the types of OMPs and produced TPs are different in various AOP (Yang et al., 2017; Zhang et al., 2016), it would be important to investigate the reaction mechanism of OH• (as a major oxidant in AOP) with major structure of OMPs (e.g., aromatic structure, olefines, amines) to understand the fundamental mechanism of TPs formation.

Detection of TPs in the laboratory-based study is the first and most important step to investigate the formation mechanisms of TPs. A number of studies have developed analytical techniques to identify the TPs, such as the liquid chromatography (LC) coupled with high-resolution mass spectrometry since the early 2000s[86]. Yet, the analytical methods used in the detection (such as liquid chromatography-mass spectrometry and nuclear magnetic resonance) come with some limitations. For example, while the precision of the method has been significantly improved by using an updated version of the equipment, the application of analytical methods can be still constrained by the unavailability of the TPs standard[87].

Furthermore, it takes an enormous amount of manpower and time to experimentally examine the innumerable OMPs and TPs[14,87]. Considering the cost and human resources involved in laboratory experiments, it may not be practical to comprehensively investigate TPs not only for all chemicals currently used (over 100,000 chemicals) but also for those that will be synthesized in the future. Further, if the relatively fast reaction, which may be overlooked in experimental analysis, is related to the deterioration of process efficiency (e.g., by interfering the full mineralization and forming toxic and stable TPs)[88,89], the elucidation of such reaction pathways will be important for engineering purposes.

To overcome the existing limitations of the experimental approaches, the development of theoretical calculation methods and its application can be considered as a complementary or alternative approach. In particular, quantum chemical calculation (QCC) can serve as a potentially useful method to investigate the reaction kinetics and mechanisms in terms of TPs formation for a wide range of OMPs[14]. The QCC relies on the Schrödinger equation to analyse the atomic interaction in the compound molecule, including electronic structure, molecular energies, and transition state. The atomic interaction was further calculated as reactive sites using Fukui index and reaction rate constants using transition state theory for kinetic and reaction mechanism analysis. The methods for solving the equation are varied based on the level of theory such as semi-empirical, ab-initio (e.g., Hartree-Fock or HF), hybrid functionals (e.g., B3LYP and Minnesota functionals), density functional theory (DFT) and so forth. Recently, OMPs oxidation reactions are assessed using several level of theories such as M05-2X for bisphenol A[74], M06-2X for para-substituted phenolic compounds[75], Gaussian-4 theory for acetone[76], and B3LYP for ibuprofen[77]. For this study, the following three representative methods and basis sets were selected: HF, B3LYP, and M06-2X. HF is the basic and simplest ab-initio level of theory, which uses the approximation that Coulombic electron-electron repulsion can be averaged, instead of considering explicit repulsion interactions [90]. In other words, the electron correlations are not considered in HF. On the other hand, B3LYP and M06-2X are a combination or hybridization of the exact HF exchange in DFT, providing a simpler calculation for many molecular properties such as the energy of atoms, bond length, and vibration frequencies[91]. In general, the B3LYP contains approximately 20% HF exchange[92], while M06-2X has 54% HF exchange[93].

Furthermore, Minakata and Crittenden calculated the activation energies of the OH• addition to alkenes and the hydrogen atom abstraction from C-H with an accuracy of ±3 kcal/mol using Gaussian-n series (G1, G2, and G3) method and predicted reaction rate constants are within five times of the experimental values[94]. Guo, et al. expanded the number

of reactions to 101 types (e.g., addition of O_2 to carbon-centered radicals, disproportionation and single molecule decay of peroxyl radicals, etc)[95]. von Gunten's group has also conducted theoretical studies of reaction rates and pathways for ozonation of OMPs, in which OH• was produced as main oxidants for oxidation of OMPs[96,97]. It was found that the error between theoretically calculated reaction rate constants from transition state and experimental observation was from 3 to 750 times[98]. In contrast to the analysis on reaction rates, the prediction and evaluation of reaction sites provide further information on reaction mechanism, such as the electron orbitals to which oxidant reacts during the decomposition process. According to the molecular electron density theory (MEDT), molecular reactivity and reaction sites can be associated with the changes in electron density distribution in the molecule during the reaction[99]. For example, the Fukui index is potentially useful to estimate the change in intramolecular charge density during the reaction. Fukui index or Fukui function is a function that describes a chemical reactivity by analysing the electron densities in the observed molecule[100]. In recent studies, the Fukui Index has been increasingly applied to calculate the reaction sites of OMPs (e.g., pesticides and antibiotics[101–103]) with OH•. However, all these studies are limited only to the analysis of reaction sites of the OMPs, and the applicability of the Fukui Index to the reaction mechanism and resultant TPs formation is still a challenge.

To overcome this issue, we employed the Fukui Index and transition state theory to investigate the reaction mechanisms (reaction sites and rates) and resultant TPs formation during OH•-mediated phenol oxidation process. Specially, the initial stages of phenol oxidation by OH• was selected in our calculation based on the following considerations. First, the unambiguous experimental knowledge of the relevant reaction mechanisms for the initial stages of OH•-mediated phenol oxidation[104,105] allows us to rigorously examine the applicability and limitations of the QCC theoretical approach. Second, phenolic functional groups account for the majority of OMPs[75], and OH•-mediated oxidation is commonly involved in AOPs. In the calculation of reaction site, the reactivity of each carbon atom within an organic molecule was assessed, and the accuracy of the prediction was compared by using different levels of theory (Hartree-Fock, B3LYP, and M06-2X). In addition, kinetic rate constant was determined via optimization of transition state structure, and thereby the applicability and limitation of QCC theoretical approach in the kinetic analysis were discussed. Thus, this study provides a promising strategy to elucidate the fundamental kinetics and reaction mechanisms of OH•-mediated phenol oxidation, which promotes the assessment and development of AOPs for removal of OMPs in water environment.

Additionally, our outcomes contribute to accurately predicting TPs formation from the oxidation of OMPs and understand the fate of OMPs in water and wastewater treatment processes.

II.2. Methods

II.2.1. Overall Computational Procedure

Figure II-1 shows the strategy used in this study to assess phenol oxidation pathways. First, optimization of the molecule structure was conducted to obtain the base structure for further calculations. In this step, a conformational analysis was also carried out (prior to the structure optimization) to find the major isomers. Then, the optimized structure underwent a Fukui index calculation to find the most reactive site and to yield an estimation of the product structure at the end of the reaction. Subsequently, the product structure was built, underwent conformational analysis, and optimized again. The obtained reactant and product structures were used as an input to find a transition state (TS) structure. If the TS structure fulfils the criteria (described later in next section), activation energy was calculated and so does reaction rate constant. The cycle was also repeated for all reactions considered in this study.

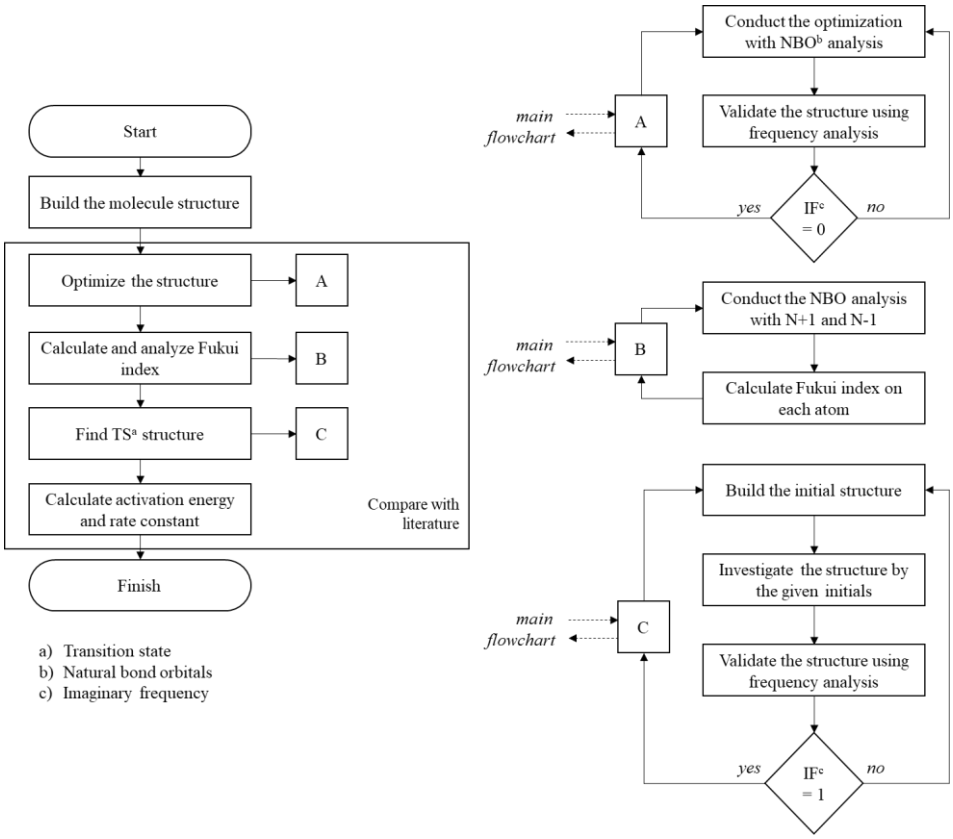

Figure II.1 Flowchart of calculation steps for each pathway

Table II-1 Previously theoretical researches on OMPs in AOPs system

Target organics	Oxidants	Medium	Calculation Method	Level of Theory	Basis set	Solvent effect	Reaction mechanism	Calculated parameters	References
Phenol	$OH^{\bullet}$	Water	TS, Energy	HF B3LYP M062X	6-311+G(2d,2p) 6-311+G(2d,2p) 6-311+G(2d,2p)	SMD	OH addition O_2 addition HO_2 dissociation	Fukui function Free energy of activation Second order rate constant	This study
Bisphenol A	$OH^{\bullet}$	Water	TS	M052X	6-311++G(d,p)	SMD	H-abstraction	Second order rate constant	[74]
Ibuprofen	$OH^{\bullet}$	Water	TS	B3LYP	6-311++G(d,p)	PCM	H-abstraction	Second order rate constant	[77]
Organic compounds (n=31)	$Cl^{\bullet}$	Water	TS, Energy	B3LYP	6-31G(2df,p)	Implicit PCM	H-abstraction, Cl^- adduct formation	Free energy of activation	[106]
Acetone	$OH^{\bullet}$	Water	TS, Energy	Gaussian-4 theory	Gaussian-4 theory	SMD	Significant involvement of $OH_2^{\bullet}$ in peroxyl radical reaction	Free energy of activation	[76]
Para-substituted phenolic compounds	O_3	Water	TS, Energy	M062X	6-311+G(2d,2p)	SMD	Formation of p-benzoquinone, p-substituted catechol, cyclic α,β-unsaturated ketone	Free energy of activation and reaction	[75]
Glutathione	$OH^{\bullet}$	Water	TS, Energy	M052X	6-311+G(d,p)	SMD	H-transfer (abstraction)	Second order rate constant	[107]
Naproxen	$OH^{\bullet}$	Water	TS, Energy	M052X	6-311++G(d,p)	SMD	$OH^{\bullet}$ adduct formation	Second order rate constant	[108]
Carboxylated and hydroxylated benzene (n=16)	$OH^{\bullet}$	Water	TS, Energy	M062X	aug-cc-pVDZ	SMD	$OH^{\bullet}$ addition to benzene ring producing hydroxycyclohexadienyl radicals	Free energy of activation	[109]

PCM: Polarizable continuum model, SMD: solute electron density implicit solvation model, TS: Transit

II.2.2. Molecular Structure Optimization

In the structure optimization step, equilibrium structure is estimated by determining a minimum point on the potential energy surface of the molecule. Since multiple conformational isomers can occur for the target molecular structure, the structural optimization converges to either local or global minimum, depending on the initial structure coordinate. Therefore, in order to obtain the lowest energy among the possible isomers, the most stable conformation was searched using CONFLEX 8[110] and used as the initial coordinate.

Then, molecular structure optimization was performed using Gaussian 16 revision B.01[111] and GaussView 6[112]. Regarding the computational method, the level of theory and basis function used in previous studies on the radical-mediated reactions of various organic molecules were listed in Table II-1. The representative degree of accuracy and cost of each level of theory is shown in Figure S1. Among them, the following three representative methods and basis sets were selected in this study: HF/6-311+G(2d,2p) (ab-initio), B3LYP/6-311+G(2d,2p) (hybrid functionals), and M06-2X/6-311+G(2d,2p) (hybrid functionals). To simulate the reaction in an aqueous phase, an implicit solvation model named SMD (Solvation Model based on Density)[113] was used. SMD is a continuum solvation model based on quantum mechanical charge density, which takes into account the electrostatic interaction between solute and solvent using Poisson's equation and the short-range interaction between solvent and solute in the first solvation shell due to the cavity structure of the solvent[113].

II.2.3. Calculation of Reaction Site using Fukui index

Fukui index (or Fukui function) was employed in this study to estimate the most reactive site of phenol and its TPs. Fukui index generally determines the regioselectivity of a molecule to a certain reaction using the variable f(r), which suggests the potentially most reactive site[100]. The variable f(r) is depicted in Equation 1 as follows:

$$f(r)=d\rho(r)/dN \quad (1)$$

where f(r) is Fukui index, ρ(r) is electron density of a certain atom, N is total number of electrons in the molecule. To predict the site-favoured reactivity of a molecule, the index was calculated by using Equations 2 to 4 as follows:

$$f^{+}(r)=\rho_{N}(r)-\rho_{N+1}(r) \quad (2)$$

$$f^{-}(r)=\rho_{N-1}(r)-\rho_{N}(r) \quad (3)$$

$$f^{0}(r)=0.5\left(\rho_{N-1}(r)-\rho_{N+1}(r)\right) \quad (4)$$

Equation 2 is for nucleophilic reaction, where the total number of electrons in the molecule increased by one; Equation 3 is for electrophilic reaction (total number of electrons in the molecule decreased by one), and the last Equation 4 is for a radical attack[114]. We assumed that the higher the index value of a site, the more likely the site is a site-favoured reactivity.

In the calculation of the Fukui index, the structure was optimized in the reference state (i.e., $\rho_N(r)$) by Gaussian 16, and then the populations (electron densities) were analysed by changing the number of electrons and spin multiplicity. Since Mulliken's populational analysis is sensitive to various properties such as the basis functions, quantum mechanical methods, and molecular structure itself[115,116], the natural population analysis (NPA) was adopted in this study to calculate the atomic charges and orbital populations. Thus, Fukui index is a measure of the change in the electron density of an atom when an electron is added or removed from a certain potential. In the frontier orbital theory, such additional electrons are added to the LUMO and removed from the HOMO orbital. In a previous study, Elhorri et al.[117] identified the reaction point (radical reaction to nitrogen atom) for the initial structure of dye (e.g., blue acid) with OH• by Fukui index, and the calculation showed comparable output to experimental observation. The Fukui index was also applied to the reactions of radicals with pesticides (e.g., atrazine[118]) and antioxidants (e.g., flavonoids[119]) for each initial structure, indicating the applicability of Fukui index in diverse radical reactions.

II.2.4. Optimization of Transition State Structure

Optimization of transition state for specific reaction was initially performed by the quantum computational chemistry software Reaction plus Pro 2 (HPC systems)[120]. In this calculation, the geometric structure of the transition state is searched based on the Nudged Elastic Band (NEB) method[121] using the starting and ending states as input data. In this method, about 5-15 molecular structures (beads) are placed at equal intervals on the reaction coordinate axis where products are formed from reactants, and each molecule is connected with a string to search for the reaction path with the lowest energy on the reaction potential surface. The saddle point of the energy obtained by this search is considered the transition state. This first (relatively rough) estimation of TS structure using Reaction plus Pro 2[120] was followed by rigorous optimization using Gaussian 16 with validation by frequency analysis and intrinsic reaction coordinate (IRC) validation. In this study, it is assumed that the electron transfer in the product molecule is fast, and that the stabilization of the molecular structure occurs more quickly than in an external molecular transfer reaction.

II.2.5. Kinetic Rate Constant Calculation

The activation energy of a certain reaction is highly related to the transition state geometry of the reactants and the products (i.e., Transition State Theory (TST) or activated-complex theory)[90]. The idea of the theory is based on a molecular collision that leads to a reaction that must pass through an intermediate state as transition state. Using activation energy ($\Delta G^{\ddagger}$) representing the energy difference between the TS structure (structure that lies in the transition state) and reactants, the reaction rate constant can be calculated using Equation 5[90]; i.e.,

$$k(T)= \frac{k_B \cdot T}{h \cdot C} \exp\left(-\frac{\Delta G^{\ddagger}}{R \cdot T}\right) \quad (5)$$

where k is reaction rate constant, k_B is Boltzmann constant (1.381×10^{-23} $J\cdot K^{-1}$), T is temperature (K), h is Planck constant (6.63×10^{-34} $J\cdot s$), C is concentration of the molecule (unit $mol\cdot L^{-1}$), R is ideal gas constant (8.314 $J\cdot K^{-1}\cdot mol^{-1}$), and $\Delta G^{\ddagger}$ is activation energy ($J\cdot mol^{-1}$).

II.2.6. Initial Oxidation Process of Phenol

In this study, we focused on the initial oxidation process of phenol to hydroquinone or catechol. The reactions are experimentally well defined as noted in literature[104,105] (Figure II-2). The reactions consist of Path c1 to c3 for catechol production pathway and Path h1 to h3 for hydroquinone production pathway, where seven structures can be involved; i.e., phenol (PH), ortho-dihydroxylhexadienyl radicals (o-DHCH), ortho-peroxyl radicals (o-DHCH.O_2), para-dihydroxylhexadienyl radicals (p-DHCH), para-peroxyl radicals (p-DHCH.O_2), catechol, and hydroquinone. Path 1 is a radical reaction where OH• is added to phenol. Path 2 is an electrophilic reaction where dissolved oxygen (O_2) is added to DHCH to form peroxyl radical (DHCH.O_2). Path 3 is a radical reaction where hydroperoxyl radical (HO_2•) is dissociated from DHCH.O_2 to form hydroquinone or catechol. In the oxidation of phenol in water, phenolate (e.g., pKa = 9.95) is considered to be dominant near neutral pH[107], but for the reaction with OH•, phenol is also highly reactive and is considered a major reactant[105].

It had been observed that the hydrogen abstraction reaction occurred in hydroxyl radical reactions with aromatic compounds, for example a study of aromatic amino acids (enthalpy barriers obtained in the range of 4.1 to 6.7 kcal/mol) [122] as well as benzoic acid (4.27 kcal/mol) [123]. The result from those studies confirmed that hydrogen abstraction is a possible reaction mechanism in OH radical attack to the aromatic compounds, but the reaction is less favorable thermodynamically compared to OH radical addition (-1.0 to 1.0 kcal/mol for

aromatic amino acids and 1.97 to 2.59 kcal/mol for benzoic acid). Therefore, OH radical addition reaction to phenol will be the focus of this study for the first oxidation stage.

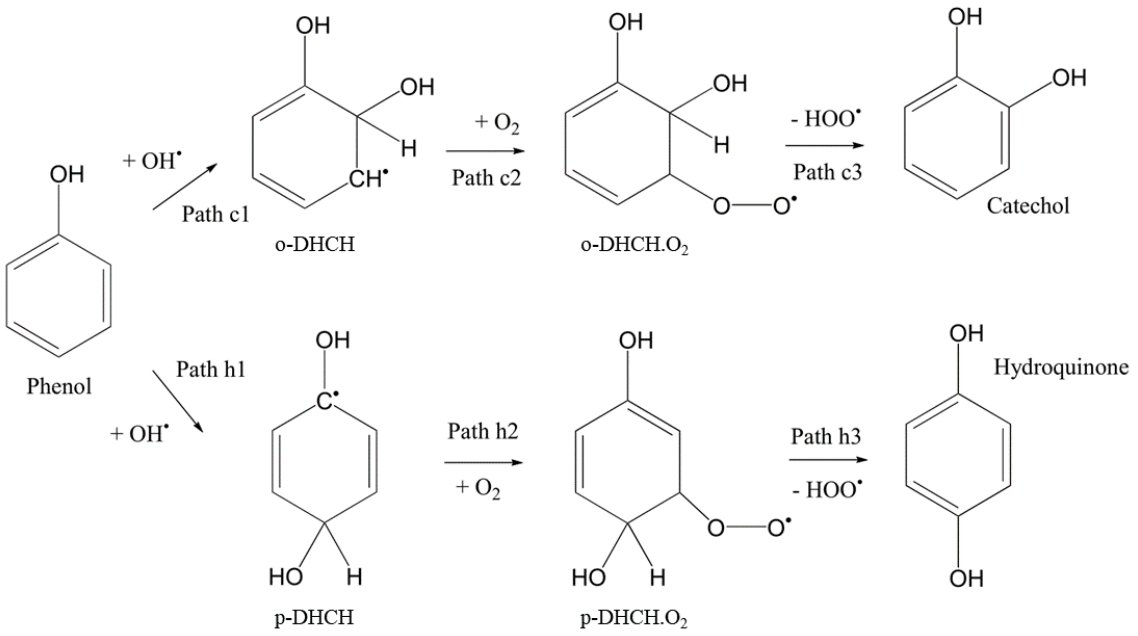

Figure II.2 Phenol oxidation pathway with hydroxyl radical adapted from the literature[104,105].

II.3. Results and Discussion

II.3.1. Structure Optimization for Phenol

Among all molecules involved in the initial stage of phenol oxidation, the structure of phenol has been rigorously determined by experimental analysis[124]. Therefore, as a first step, the phenol structure was calculated using HF, B3LYP and M06-2X and all calculated results were compared to the experimentally determined structure information reported in literature. In Table 1, the prediction accuracy of the calculated structure including bond lengths and angles was listed for the level of theories employed. The highest root-mean-square error (RSME) against the literature value was obtained for HF, which accounted for 0.013, indicating that calculation with HF had the largest difference from the experimentally determined value. Among the methods used, B3LYP showed the lowest RSME (0.004), and M06-2X (0.007) calculation resulted in slightly larger RSME than B3LYP.

Table II-2 Calculated bond lengths and angles of phenol structure in this study in comparison with the literature[124].

Element	Bond length (Å)			
	HF	**B3LYP**	**M06-2X**	**Measured value[124]**
C1-C2	1.382	1.391	1.388	1.394-1.397
C2-C3	1.385	1.393	1.391	1.395-1.397
C3-C4	1.383	1.393	1.390	1.395-1.397
C4-C5	1.384	1.392	1.389	1.392-1.397
C5-C6	1.384	1.393	1.390	1.391-1.397
C6-C1	1.384	1.393	1.390	1.391-1.398
C6-O	1.359	1.381	1.372	1.364-1.398
O-H	0.944	0.965	0.964	0.953-0.957
RMSE	**0.013**	**0.004**	**0.007**	
Element	**Bond angle (°)**			
	HF	**B3LYP**	**M06-2X**	**Measured value[124]**
C1-C2-C3	120.73	120.64	120.62	120.48-120.57
C2-C3-C4	119.17	119.37	119.37	119.74-119.75
C3-C4-C5	120.72	120.58	120.59	120.79
C4-C5-C6	119.46	119.44	119.44	119.22
C5-C6-C1	120.44	120.56	120.54	N/A
C6-C1-C2	119.49	119.41	119.45	118.77-119.43
C6-O-H	110.87	109.53	109.62	106.40-109.00
RMSE	**1.33**	**0.79**	**0.82**	

The results of bond length and angle calculations could be elaborated by the findings of Bushnell and Gauld[125]. The authors compared a range of the level of theories for nonheme iron enzyme 8R-LOX—a metalloenzyme that catalyses various metabolically important reactions within an organism such as C-H bond activation, hydrolysis, and DNA repair—and found that B3LYP has a similar accuracy with M06 level of theory in terms of optimization of molecules. On the other hand, the results from the HF level of theory might be a direct consequence of maintaining full configuration interaction that mostly produces a smaller bond length than the experimental observation[90].

In this study, the other structures along the pathways including o-DHCH, p-DHCH, o-DHCH.O_2, p-DHCH.O_2, catechol and hydroquinone were also optimized. It should be noted,

however, that because there are no available data (to our knowledge) on the experimentally measured bond properties of such molecules, the comparison was made only for phenol structure in this study.

II.3.2. Prediction of Reaction Site

(i) OH• Addition Reaction (Path h1 and c1)

Organic compounds such as aromatic and aliphatic compounds and alkenes have been recognized to produce carbon-centred radicals (i.e., DHCH in this case) by the addition of OH• to unsaturated carbon bonds of benzene rings and alkenes, or by hydrogen atom abstraction [126]. In case of phenol, reaction with OH• yields DHCH molecule as carbon-centred radical, as depicted in Figure II-2. In this OH• addition reaction (i.e., Path h1 and c1), the Fukui index was calculated for optimized phenol structure using all methods (Table S2 in Supporting Information), showing that the ortho-positioned carbon (C-1 and C-5) especially C-1, had the highest Fukui index value, followed by para-positioned carbon (C-3). Meanwhile, negative values were produced in the ipso-positioned (C-6) and meta-positioned (C-2 and C-4) carbon. The negative value of a certain site in Fukui index generally suggests that the relevant site is not involved in the reaction [127]. Overall, the Fukui index results indicated that the most reactive site of the phenol for OH• addition reaction is C-1, followed by C-5 (ortho-positioned carbon same as C-1), and C-3 (para-positioned carbon).

To further interpret the likelihood of reaction more quantitatively, branch ratio (shown in %OH• addition in Table 2) of each position was calculated and compared with the experimental observation[32,104,105]. More specifically, this ratio was calculated by dividing the index value of each carbon atom to the sum of the Fukui index values for all six carbon atoms in the phenol molecule. The negative index values were not considered; e.g., the ratios were assumed to be null for ipso-positioned and meta-positioned carbons in the calculation of OH• addition reaction.

According to the calculation result of %OH• addition (Table 2), M06-2X produced a 77% ratio for ortho-positioned and 23% for meta-positioned carbon. This result was comparable to the previously reported experimental values, where a branch ratio of approximately 70-80% was obtained for ortho-positioned carbon and 20-30% for para-positioned carbon[32]. The same report indicated that the reaction for meta- and ipso-position carbons is negligible, consistent with M06-2X calculation (i.e., 0%) in this study. The other studies reported that reaction with meta- and ipso-positioned carbons occurs albeit its branch ratio is small (e.g., less than 8%)[104,105]. Regarding the other calculation methods, HF and

B3LYP showed substantially different results compared to the experimental observation: e.g., the branch ratio for both ortho-positioned carbon (99% in HF and 91% in B2LYP) was overestimated and that for para-positioned carbon was underestimated (1% in HF and 9% in B2LYP) as shown in Table 2.

Table II-3 Calculated branch ratio for OH• radical attack of phenol (%OH• addition) based on the optimized structure in this study with the literature values as comparison

Reaction site(s)	Calculated %OH• addition			Experimental %OH• addition		
	HF	B3LYP	M06-2X	Stefan[105]	Mvula, et al[104]	Alnaizy and Akgerman[32]
ipso (C6)	0	0	0	8	0	N/A
ortho (C1 and C5)	99	91	77	50	63	70-80
meta (C2 and C4)	0	0	0	8	7	N/A
para (C3)	1	9	23	34	30	20-30

(ii) Reactions for DHCH and DHCH.O_2 (Path h2-h3 and c2-c3)

After DHCH is generated by OH• addition to phenol (Path c1 and h1), DHCH subsequently forms a complex in the presence of O_2, producing peroxyl radicals (i.e., DHCH.O_2 via Path c2 and h2). Both o-DHCH.O_2 and p-DHCH.O_2 can be formed, when the oxygen molecule is bonded to the adjacent carbon that is attacked by OH• (Figure II-2). This pathway can be considered an electrophilic reaction, because O_2 is a nucleophilic molecule having two lone pairs of electrons, leaving the DHCH molecule an electrophilic. After O_2 molecule is added in the molecule, the reaction can be followed by catechol or hydroquinone formation via dissociation of HO_2• molecule from DHCH.O_2 (Path c3 and h3), which is considered as a radical reaction. These reaction pathways have been shown qualitatively in previous studies based on experimental observations[104,105], but to the best of our knowledge, no study has experimentally determined the branch ratios for Path c2, h2, c3, and h3. In this study, the values of Fukui index were calculated for molecules involved in the reaction pathway to verify the consistency between theoretical calculations and experimental observations, and to examine the applicability of theoretical calculations.

For hydroquinone production pathways, the calculation for the p-DHCH molecule indicated that all three methods yielded substantially different values for Fukui index (Table S3 in Supporting Information), and therefore different predictions for the reaction sites in Path h2. For example, HF yielded only one positive value for C-3, so the branch ratio for this

reaction site was 100% for C-3. As can be seen in Table S3, however, C-3 already had four bonds with other atoms. Thus, the reaction probability of C-3 occupied by other bonds should be extremely low, which is inconsistent with HF calculation. Also, the B3LYP calculation yielded no positive value, resulting in a branch ratio of 0% for all carbon atoms. This result generally indicates that the reaction did not take place, which is indeed inconsistent with the previous finding showing the significant formation of peroxyl radicals via this reaction pathway [104]. Contrary to the above two methods, in M06-2X, the branch ratios were calculated to be 61% and 39% for meta- and ipso-positioned carbons, which is consistent with the previous findings in the literature (Fig 2). Therefore, compared to HF and B3LYP, M06-2X showed better performance in terms of prediction of p-DHCH reaction site in Path h2.

For Path h2, C-6 actually had the highest branch ratio (39%): therefore, O_2 could be added to C-6 to form p-DHCH.O_2. The O_2 molecule on C-6 subsequently reacts with the H atom (H-9) bonded to C-3 to form HO_2•, and catechol can be formed via further reaction intermediates [105]. However, the H-9 atom and the O_2 molecules (O-16 and O-17) on C-6 in p-DHCH.O_2 are spatially far apart, as such the reaction is unlikely to proceed quickly in view of steric perspective. On the other hand, when an oxygen molecule (O-16, O-17) is added to C-4, the oxygen molecule locates sufficiently close to the hydrogen atom (H-8) of C-2 for the p-DHCH.O_2 dissociation reaction to occur. In this study, therefore, we considered that the latter reaction pathway, which does not involve further reaction intermediates, is significant. The identical steric issue is expected to be the case for catechol production pathways (i.e., Path c3).

In the dissociation reaction of p-DHCH.O_2 (Path h3), therefore, HO_2• can be formed via binding of two oxygen atoms (O-16 and O-17) in C-4 and one hydrogen atom (H-9) in C-3. For this pathway, only HF (displayed in Table S4 in Supporting Information) yielded an inconsistent result with the experimentally observed pathway. It is possible that HF produce a deviated value due to its nature of neglecting electron correlations in the molecule [90]. The branch ratios from B3LYP and M06-2X consistently indicated that C-3 and C-4 are the most reactive sites in this radical reaction, which is comparable to the experimental observation. In addition to the Path 3, it is known that peroxyl radicals (L-O_2•, where L is an organic molecule) can produce various intermediate radicals (e.g., alkoxyl radicals [L-O•]) and TPs (e.g., alcohols, ketones, and aldehydes) via complex reactions such as unimolecular decay or bimolecular disproportionation reactions[76,126], which can further react with OH• to form carboxylic acids. Given that the ring-opening reaction of aromatic can be driven by peroxyl

radicals, it will be important in future studies to investigate the applicability of QCC to more complex radical and ring-opening reactions.

Similar to hydroquinone production mechanism, the calculation of catechol production pathways (Path c2 and c3) generated the branch ratios for o-DHCH and o-DHCH.O_2 molecules, as listed in Table S5 and Table S6 in Supporting Information. According to Table S5, all level of theories showed the highest ratio for C-4, followed by C-2 in case of o-DHCH. However, due to aforementioned steric issue noted for the Path h2, C-4 was not considered as a possible electrophilic reaction site, since it has a significant distance to further react with C-1 to produce catechol. Instead, we considered C-2 as the reaction site for Path c2, which has the second highest branch ratio and adequate distance to C-1.

Regarding the branch ratios for o-DHCH.O_2, which depicted in Table S6, HF results substantially differed from both B3LYP and M06-2X. For example, HF generated C-2 and C-3 atom as the potential reaction sites for HO_2• dissociation (e.g., the branch ratio for HF method was highest for C-3 [24%] followed by C-2 [18%]), while for B3LYP and M06-2X, C-1 and C-2 were suggested to be the favourable reaction sites. Given that the dissociation of HO_2• from o-DHCH.O_2 finally generates catechol as reported in literature, the dissociation should occur from the O_2-attached (C-2) and OH•-attached (C-1) carbons, and both B3LYP and M06-2X agreed with the experimental observation.

II.3.3. Kinetic Rate Constant

(i) Transition State Structure Identification

In order to better understand the mechanisms of reactions, detailed investigation on the transition state (TS) structure and intrinsic energy was conducted. Given its best performance in the Fukui index calculation, M06-2X was selected to find the transition state structures and calculate the activation energy ($\Delta G^{\ddagger}$) of each pathway. Finally, the activation energy ($\Delta G^{\ddagger}$) was used to calculate the reaction rate constant of each pathway followed by comparison with the reported rate constants.

In the search for a transition state, we found four transition state structures along the pathway, namely Path h2, h3, c2, and c3. No transition state structure was detected for Path h1 and c1. Since OH• is highly reactive, most reactions with this radical would not produce a transition state[105]. The absence of a transition state may also be relevant to the quantum tunnelling phenomenon of electrons, where electrons are transferred without an energy barrier and thus transition state structures are not formed[90]. Moreover, a low lying TS may not be detected if the potential energy surface from the neighbouring molecules is shallow

due to the low computational load without explicit solvation[128]. Hence, we investigated four transition state found along each pathway (TSh2 and TSh3 for hydroquinone and TSc2 and TSc3 for catechol), as shown in Figure II-3. The vibrational frequency analysis showed that all detected structures had one imaginary frequency and the IRC validation also further confirmed the connection between found TS structures and their respective reactants and products.

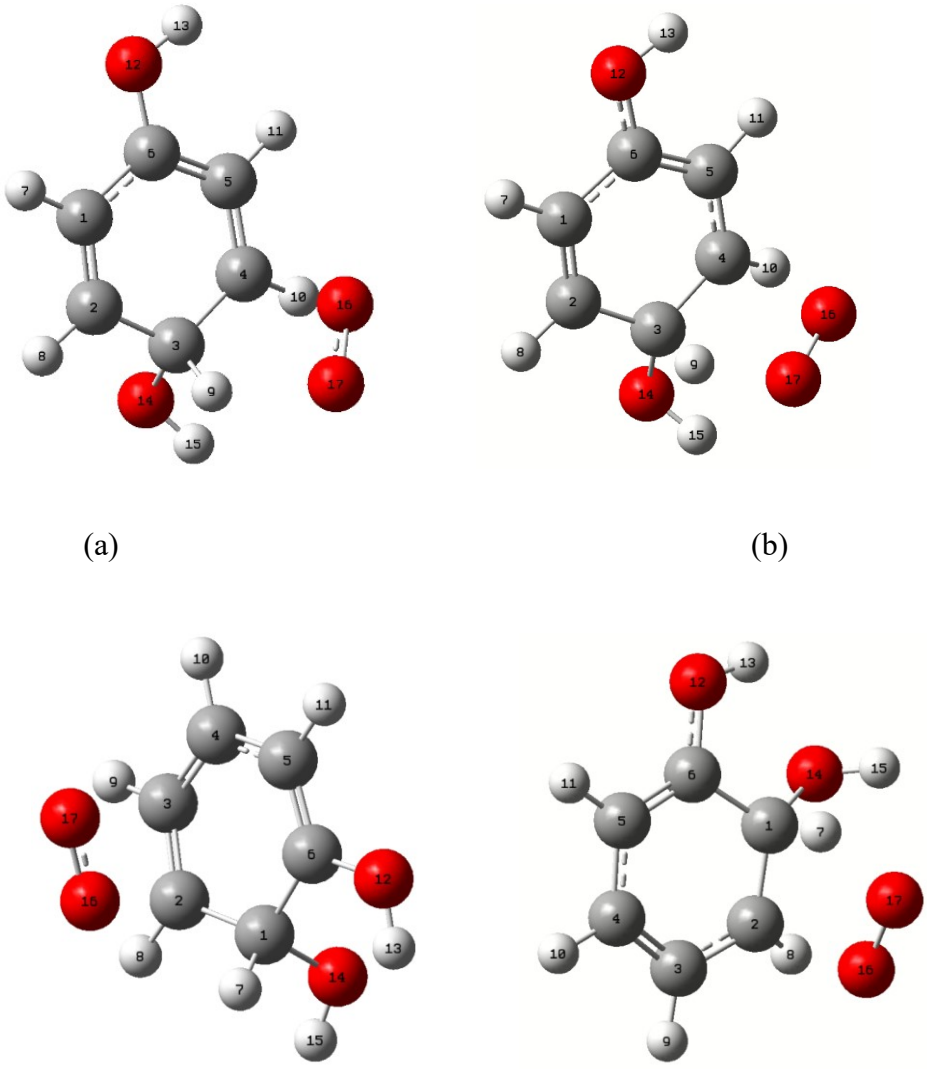

(a) (b)

(c) (d)

Figure II.3 Calculated TS structure for Path h2 (a), Path h3 (b), Path c2 (c) and Path c3 (d)

(ii) Activation Energies and Reaction Rate Constants

The intrinsic energies of the TS structures were calculated, and then the activation energies and reaction rate constants (k) of Path h2, h3, c2, and c3 (Figure II-4 and Table 3), were compared to the reported theoretical and experimental results. The calculated k of Path h2 was 2.8×10^{11} $M^{-1} \cdot s^{-1}$, which was several orders of magnitude greater than the calculated k for Path h3 (1.4×10^{2} $M^{-1} \cdot s^{-1}$). Similarly, k for Path c2 (1.43×10^{10} $M^{-1} \cdot s^{-1}$) was also considerably larger than Path c3 (1.41×10^{2} s^{-1}). Thus, Path c3 and h3 can be the rate-limiting steps of the pathways which is consistent with the reported experimental evidence[104]. The calculated results also showed that Path c2 and h2 (in addition to Path c1 and h1 where no TS structures were detected) were near diffusion-controlled reactions (e.g., $\sim 10^{10}$ $M^{-1} \cdot s^{-1}$)[129], which agreed with the experimental result in the literature.

Table II-4 Calculated $\Delta G^{\ddagger}$ and k of each pathway as well as their comparison with the reported values in the literature

Path	**$\Delta G^{\ddagger}$ (kJ/mol)**	**Calculated k_i (T = 298.15 K)**	**Theoretically reported k_i**	**Experimentally reported k_i**	**Experimentally reported $k_{overall}$**	**Unit**
c1	-	-	6.28×10^{9}[a]	$(0.841 \pm 0.042) \times 10^{10}$[b]	6.51×10^{6}[d]	$M^{-1}.s^{-1}$
c2	15.06	1.43×10^{10}	-	1.490×10^{9}[b] 1.200×10^{9}[c]		$M^{-1}.s^{-1}$
c3	61.52	1.20×10^{1}	-	0.438×10^{5}[b] 1.300×10^{5}[c]		s^{-1}
h1	-	-	1.98×10^{9}[a]	$(0.841 \pm 0.042) \times 10^{10}$[b]	1.27×10^{6}[d]	$M^{-1}.s^{-1}$
h2	7.68	2.80×10^{11}	-	1.490×10^{9}[b] 1.200×10^{9}[c]		$M^{-1}.s^{-1}$
h3	61.93	1.41×10^{2}	-	0.438×10^{5}[b] 1.300×10^{5}[c]		s^{-1}

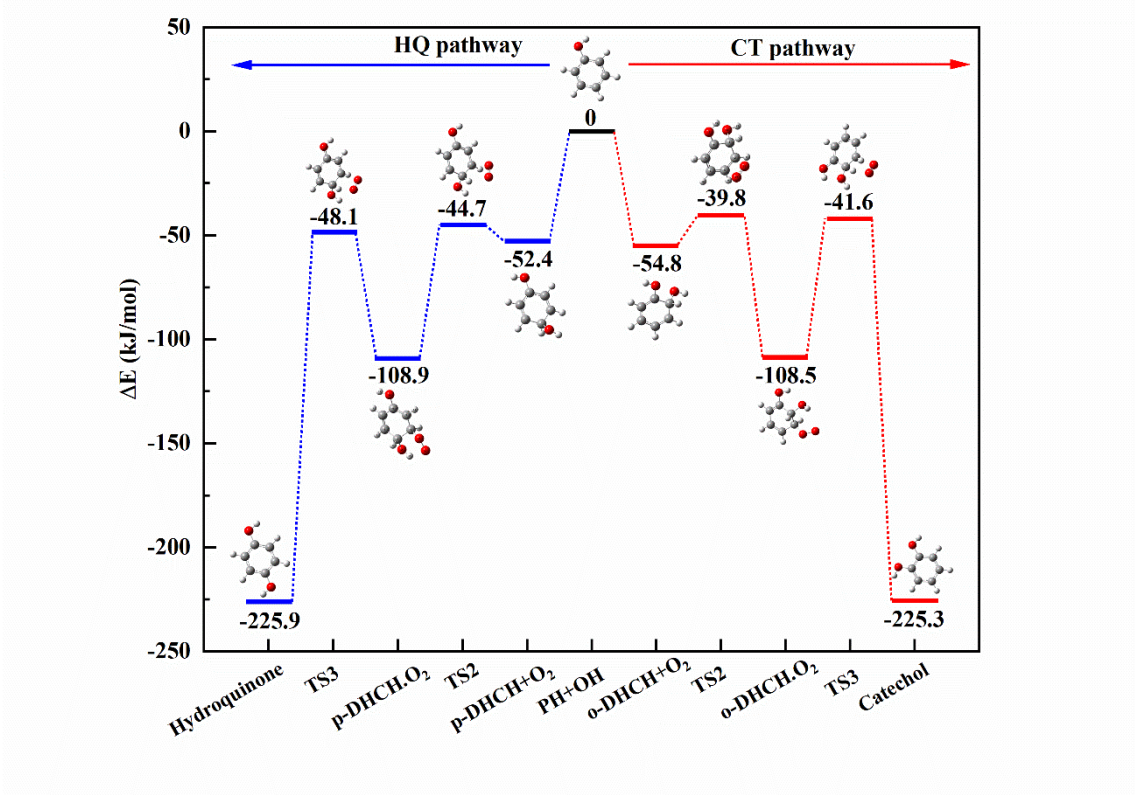

Figure II.4 Energy profile of phenol oxidation pathway to catechol and hydroquinone relative to phenol.

A comparison to the experimentally reported values revealed that calculated k for Path c2 and h2 differed from the reported k value by a factor of 10^1 to 10^2, whereas the calculated k for Path c3 and h3 differed significantly (by 10^3 to 10^4-folds) from the reported k. The overestimation of activation energy may be one of the plausible reasons for this discrepancy. According to the previous studies, the calculated rate constant may include a large error, approximately 3 to 750 times compared to the measured value[98,130]. Other studies have also shown that the acceptable difference between theoretical and experimental results is within 3 kcal/mol (or 12.6 kJ·mol^{-1})[94,131], with a maximum of 7.6 kcal·mol^{-1} specifically for the M06-2X level of theory[132]. Such error can be attributed to the dispersion effect of catechol/hydroquinone and HO_2• in the calculation of the TS structure, which likely affects the electron density analysis, resulting in the failed description of intermolecular dispersion interaction[133]. Intervention of dispersion effect (emp=dp3) in the calculation resulted in the 6-fold increase of reaction rate constant of Path h3 (1.41×10^2 to 8.22×10^2).

Another plausible reason for such a large discrepancy is that the system has a significant multireference character that can produce imprecise results[134]. Multireference character typically occurs in molecules with challenging electronic structures, such as biradicals or diradicals, which are the molecules with two unpaired electron. In this study,

p.DHCH.O_2 and o.DHCH.O_2 are the molecules having two unpaired electrons due to the from O_2 group, therefore are categorized as having multireference character. Such case could not be accurately solved using single reference function used in current study, instead Complete Active Space Self-Consistent Field (CASSCF) and Multi-Configurational Self-Consistent Field (MCSCF) methods offer more flexible and accurate description of the electronic structure in challenging molecular systems.

Furthermore, according to the study by Kirklin et al[135], there may also be an analytical error in determining the kinetic rate constant from the experiment, which is estimated to be approximately 0.082 eV/atom (7.9 kJ·mol^{-1}/atom). This experimental error is comparable to those observed between theoretical and experimental results (e.g., 0.057-0.116 eV/atom or 5.5-11.2 kJ/mol/atom). The literature used for the comparison in this study employs pulse radiolysis to measure the reaction rate constant, which involves potential errors, as described in the study[136,137].

In the computational method used for transition state in this study, M06-2X was employed. The Minnesota functionals such as M06-2X are considered an effective function for weak interactions such as pericyclic reactions[138]. Xiao et al.[74] theoretically calculated the reaction rate constant for the initial reaction of endocrine disruptor (bisphenol A) with OH• using M052x/6-311++G(d,p). The reaction rate constant was estimated to be 1×10^{10} $M^{-1}\cdot s^{-1}$, with the assumption that the hydrogen abstraction reaction at the aromatic ring is most likely to occur. This value is relatively close to the experimental value of 7×10^{9} $M^{-1}\cdot s^{-1}$ (pH 7.6). Nonetheless, it is also recognized that hybrid functionals tends to underestimate the activation energy, and if hybrid functionals is not accurate enough for the TS optimization, the MP2 or CCSD method should be considered. However, while the computational cost of HF and hybrid functionals is proportional to n^3 to n^4 (where n is the number of electrons in the system), the computational cost of MP2 and CCSD methods is proportional to n^5 to n^6, indicating that the computational cost increases by a factor of up to n^3. In this study, we used a workstation (Intel Xeon/2.1 GHz/RAM 128GB), and the calculation of the TS optimization by M06-2X took about 72 hours.

II.4. Conclusions and limitations

This study investigated the accuracy of theoretical calculation using QCC in predicting the reaction mechanism of the OH•-mediated phenol oxidation (where catechol and hydroquinone are generated as TPs). First, B3LYP provided the most accurate result of

structure, followed closely by M06-2X. However, M06-2X performed the best in reactive site prediction compared to B3LYP and HF, thus M06-2X was further used in the next calculation steps. Next, the calculated results of the transition state structures and activation energies showed an agreement with the experimentally determined values for Path c2 and Path h2 (O_2 addition). In contrast, there was a gap in Path c3 and Path h3 (HOO• abstraction), implying either the limitation of theoretical calculations (which does not consider dispersion effect and multireference character in the calculated system) or discrepancies potentially caused by experiment (including analytical errors and discrepancies of target reactions between experiments and theoretical calculation).

Further studies examining Path c3 and h3 considering those factors are important to minimise the gap between experimental and theoretical studies. Also, other reactions need to be studied, such as ring-opening reactions that can occur after pathways c3 and h3. Ring-opening reactions are key reactions that lead to the mineralization of aromatic compound. Another research direction would include the oxidation reactions with other major chemical moieties (e.g., functional groups), such as benzenes, olefins, and amines. These approaches will provide better insights into the occurrence and fate of TPs in the AOPs system.

II.5. Acknowledgements

This study was financially supported by JSPS Kakenhi (19K21986, 20F20044).

CHAPTER III Interpretable Machine Learning and Reactomics Assisted Isotopically Labelled FT-ICR-MS for Exploring Reactivity and Transformation of Natural Organic Matter During UV Photolysis

Related publication:

Dwinandha, D., Gao, R., Fu, QL., Liu, J., Elsamadony, M., Fujii, M. 2023. Interpretable Machine Learning Assisted Isotopically Labelled FT-ICR-MS for Exploring Natural Organic Matter Reactivity and Its Molecular Changes During UV Photolysis. (**Submitted**)

III.1. Introduction

Ultraviolet based advanced oxidation processes (UV AOPs) have gained attention as techniques for efficiently breaking down stubborn pollutants and disinfecting water. They are popular, due to their installation, operation and maintenance well as their ability to tackle chlorine resistant pathogens. However the presence of matter (NOM) in the source water poses a significant challenge to the effectiveness of UV AOPs in degrading pollutants. This occurs because UV radiation interacts with NOM in ways leading to a decrease in UV induced degradation efficiency. These interactions result in effects such as hindering radical generation scavenging produced radicals during the process and promoting the formation of potentially harmful transformation products and disinfection by products. To understand NOM reactivity better researchers have employed strategies including analyzing its response to UV irradiation using techniques like UV spectroscopy and fluorescence measurements. These studies have revealed that NOMs reactivity towards UV irradiation depends on the applied UV dose; higher doses can cause changes such as depletion of chromophoric structures alterations, in weight and hydrophobicity and carbon removal. Furthermore researchers have also investigated the responsiveness of chemical compounds that resemble matter (NOM) which has provided valuable information, about various reaction mechanisms. These mechanisms involve electron transfers, substitution of hydroxyl radicals, cleavage of rings and ultimately mineralization processes.

Recent studies have turned to high-resolution mass spectrometry, namely electrospray ionization Fourier transform ion cyclotron resonance mass spectrometry (ESI FT-ICR MS), to probe deeper into the molecular subtleties of NOM reactivity. Researchers have been able to investigate the chemical changes inside NOM at an unparalleled degree of detail, both in natural habitats and artificial water systems, thanks to this new approach. Studies have found that exposing NOM to UV light causes changes in certain molecular properties, such as changes in oxygen-to-carbon and hydrogen-to-carbon ratios, as well as changes in the presence of certain elements such as nitrogen and sulfur. Furthermore, the use of high-resolution mass spectrometry has cleared the way for approaches such as paired mass distance (PMD) analysis, which has been useful in revealing the subtle alterations that NOM undergoes during UV-based processes. However, distinguishing between reactive and unreactive substances remains difficult, especially when they have the same molecular composition. In order to resolve these complications, isotope labeled mass spectrometry analysis has emerged as a possible avenue. This method, which employs isotopic markers, allows for accurate insights into NOM reactivity, assisting in the identification of precursor

and product formulations. This study intends to provide a deeper knowledge of NOM's behavior through a comprehensive inquiry that includes isotope labeled FT-ICR MS analysis, machine learning approaches, and PMD network analysis.

III.2. Materials and Methods

III.2.1. UV irradiation experiment

The Suwannee River natural organic matter (SRNOM) obtained from the International Humic Substances Society was prepared at a concentration of 1 g/L by dissolving it in 4 mL of deuterium oxide (D_2O) with a purity of 99.8% from Kanto Chemical, Japan, within a 5 mL quartz cell. Two sets of samples were prepared: (i) the SRNOM sample exposed to UV irradiation to simulate treated NOM and (ii) a non-irradiated sample as a control. The UV-irradiated SRNOM underwent photolysis using a photoreactor equipped with two 15-W UV lamps for 12 hours, while the non-irradiated sample was kept in the dark under the same conditions. The UV lamp intensity was set at 0.51 mW/cm2, which closely approximates the typical intensity used in individual water purification devices (0.5 mW/cm2). Buffer was intentionally excluded from the experiments to prevent the formation of radicals derived from the buffer. The pH of the NOM solutions experienced minimal change before and after irradiation (initial pH 6.2, decreased to 6.0 post-UV irradiation). To assess organic carbon concentrations, total organic carbon (TOC) analyses were performed in triplicate on both UV-treated and non-treated samples.

Following the 12-hour UV irradiation, 0.2 mL of the samples were diluted to 250 mL using ultrapure water (Milli-Q, ≥18 MΩ·cm). Subsequently, solid-phase extraction (SPE) was employed to extract dissolved organic matter (DOM). In this process, the diluted samples were acidified to a pH of around 2 using concentrated hydrochloric acid (HCl) from Kanto Chemical, Japan. The acidified samples were then passed through Bond Elut PPL cartridges (1g and 6 mL, Agilent) in a gravitational manner. Prior to use, these cartridges were activated and rinsed with 12 mL of methanol (LC-MS grade, Kanto Chemical, Japan) and 6 mL of Milli-Q water, respectively. After loading the samples onto the cartridge, a rinsing step with 20 mL of hydrochloric acid (pH ~2.0) was carried out to eliminate deuterium oxide (D2O) and labile deuterium. Subsequent rinsing with 6 mL of Milli-Q water was performed to remove any residual hydrochloric acid, followed by complete drying using nitrogen gas (99.9% purity). Finally, the samples were extracted with 6 mL of methanol and were then diluted twice using Milli-Q water in preparation for FT-ICR MS measurements.

III.2.2. FT-ICR MS analysis and formula assignment

Fourier-transform ion cyclotron resonance mass spectrometry (FT-ICR MS) stands as a high-precision analytical technique employed for accurate mass determination. Its conception traces back to the collaborative efforts of Melvin B. Comisarow and Alan G. Marshall at the University of British Columbia in 1974. In the context of FT-ICR MS, the typical process involves ionizing the sample, often through electrospray ionization. The resulting ions are then subjected to a uniform magnetic field where they are resonantly energized into coherent orbits through an excitation pulse. Following this excitation, the ions persist in their orbits at a final radius. The detection mechanism involves ions interacting with nearby electrodes, inducing the formation of an image charge on these electrodes, thereby balancing the ions' electric field. The cyclotron frequency, a key parameter, is gauged by observing the resulting "image current." Subsequently, the frequency data undergoes a Fourier transformation, yielding a mass spectrum that facilitates accurate determination of ion masses.

For the investigation at hand, both UV-treated and untreated samples were scrutinized using a 9.4T FT-ICR MS (Solarix XR, Bruker, Tohoku University). The analysis was conducted via electrospray ionization (ESI) in negative mode, utilizing a capillary voltage of -4.5 kV, an injection rate of 150 μL/h, a time domain data size of 2 million words, a measurement m/z range spanning from 150 to 1,500, and a resolution of around 200,000 (m/z = 399). The data acquisition process involved the accumulation of 50 scans. Peaks identified by the DataAnalysis software (Bruker) with a signal-to-noise ratio of 4 or higher were considered as valid signal peaks. Subsequent to data acquisition, the mass spectra were internally calibrated using a known CHO-homologous series of freshwater dissolved organic matter (DOM) within the m/z range of 200–600, employing more than 200 mass calibration points. This calibration process aimed to achieve a high mass accuracy (error less than 1.0 ppm) via FT-ICR MS. The molecular formula of the ions was determined using the FTMSDeu algorithm, which combines an existing algorithm designed for non-targeted screening of halogenated organic compounds with a novel algorithm capable of identifying deuterium-labeled mass spectra. For the neutral charge molecules detected in the negative mode ESI, the determined chemical formula was adjusted to account for a single added hydrogen atom (H). Comprehensive details of the molecular properties corresponding to the assigned formulas can be found in the Supporting Information (SI) of the study.

III.2.3. Interpretable Machine learning

A machine learning (ML) model, utilizing molecular properties derived from FT-ICR MS analysis as input descriptors, has been employed to predict specific properties of natural organic matter (NOM) associated with its reactivity in engineered systems. In contrast to previous methods, a modified approach was adopted for this study. The task involved binary classification and employed the XGBoost model, a form of gradient boosting, implemented in the R programming language. The objective was to predict whether compounds were "Reactive" (labelled as 1, indicating they had "Disappeared") or "Unreactive" (labelled as 0, also referred to as "Resistant"). The specifics of the NOM reactivity classification, including its definition, can be found in the supplementary information (SI). The ML model drew upon 15 molecular properties extracted from FT-ICR MS analysis as descriptors (as detailed in Table S1).

The dataset was divided into a 75:25 ratio, with 75% allocated for training and 25% for testing. The model's performance was evaluated using the area under the curve (AUC) value, both during tuning and for the final model. The resulting AUC value, along with a confusion matrix and a plot indicating the importance of variables, was computed based on the tuned model. Furthermore, an interpretable machine learning (IML) approach was implemented to provide insights into the model's outcomes. This was achieved through feature importance and dependence plots generated using SHAP (Shapley additive explanations), a technique that employs Shapley values to represent the contribution of individual descriptors to the model's predictions. For each formula within the dataset, Shapley values were calculated for each descriptor (in this case, the molecular properties). Subsequently, the absolute mean value of SHAP values for each descriptor across all formulas was calculated to quantify the average contribution of each molecular property. All of these methodologies were implemented using the R programming language with the SHAPforxgboost package (as outlined in code S1).

III.2.4. Paired mass distance-based network analysis

To gain insights into the primary reactions taking place within the system, paired mass difference (PMD) analysis was performed by linking precursor molecules to their resultant products. Precursor molecules were determined from the formulae identified in samples prior to UV treatment, while the products were established from the formulae solely detected post UV treatment. These precursor-product pairs were established through the calculation of mass differences, encompassing processes such as hydroxylation and

dealkylation, among others, as referenced in the supplementary information (Table S2). The visualization and analysis of the reaction network were executed using Gephi software. Further intricacies regarding the development of the network can be found in the supplementary materials.

III.3. Results and Discussion

III.3.1. Reactivity of NOM molecular compositions in UV irradiation

The photodegradation-driven mineralization of natural organic matter (NOM) exhibited modest progress after 12 hours of UV irradiation, aligning with earlier findings. While substantial TOC removal was lacking, a significant increase in molecular formulas was observed, underscoring NOM's reactivity under the UV treatment studied. Classification of precursor formulas into reactive (disappearing) and resistant (persisting) compounds revealed CHO-containing formulas as least reactive, while CHON and CHOS displayed higher reactivity. Interpretable machine learning (IML) analysis highlighted O/C ratio and molecular weight (MW) as key factors influencing reactivity across molecular compositions. In CHO-type formulas, heightened reactivity correlated with increased NOSC, lower DBE-O, and higher values of DBE-O, O/C ratio, MW, and NOSC carried notable importance values, while N-bearing CHON formulas showed significance in MW, O/C, nC, and N/C. CHOS formulas exhibited a positive relationship with S/C and negative correlation with AImod, with corresponding importance values.

Isotope labelling with deuterium (D) offered insights into OD radicals' role in photodegradation, revealing higher D-TPs proportions in CHO-TPs, and lower D-TPs in CHDON and CHDOS. Despite their reactivity, CHON and CHOS generated fewer D-TPs, potentially due to heteroatom removal, resulting in conversion to non-heteroatom molecules affiliated with CHO compounds. Notably, D-TPs from all compositions exhibited lower MW and DBE, suggesting OD radical-driven degradation.

III.3.2. Reactivity of NOM structural categories

Based on van Krevelen diagram boundaries, molecular formulas were categorized into chemical structure classes, resulting in over 5000 formulas assigned to lignin/CRAMs, tannins, condensed aromatics, carbohydrates, amino sugars, unsaturated hydrocarbons, and others. This classification aligned with previous findings that lignin and tannin-like formulas are predominant components in the studied NOM. SHAP importance values highlighted significant factors based on chemical structure classes, including heteroatom counts (nitrogen

and sulphur) and molecular weight (MW). Among these classes, specific formulas with high SHAP reactive scores contained heteroatoms such as nitrogen and sulphur, introducing functional groups like amines and sulfonic acids, enhancing reactivity by providing additional reaction sites. Notably, the reactivity of condensed aromatics was less influenced by sulphur due to limited representation, as imbalanced datasets can impact machine learning results.

Features such as MW indicated that larger molecules offer more reactive sites for photochemical reactions. Conversely, the O/C ratio held less importance in structure-based classes, highlighting its significance within identical molecular composition classes. A comparison between highly reactive and less reactive formulas within each structure category elucidated key features controlling reactivity. Reactive lignin/CRAM formulas displayed higher MW and DBE-O, indicating that larger unsaturated compounds are prone to photochemical reactions. Reactive tannin formulas exhibited higher MW, NOSC, and lower AImod, suggesting fewer oxidizable aromatics. Similarly, in condensed aromatics, high reactivity correlated with higher MW, DBE-O, DBE, and DBE/C values, while low reactivity corresponded with lower values.

Investigation into the role of OD radicals in UV reactions extended across various structural categories (Figure III-2). The transformation products (TPs) were categorized into deuterium-containing (D-TPs) and deuterium-free (D-free TPs), revealing that multiple products emerged from single precursor formulas. Specifically, lignin/CRAM, tannins, and condensed aromatics exhibited more TPs than precursor formulas, predominantly D-TPs, indicating the dominant involvement of OD radicals in the photoinduced reactions. Analysing TP features focused on D-TPs versus D-free TPs within each category, revealing patterns. D-containing TPs in lignin/CRAM had lower MW, DBE, and DBE-O values, indicating more saturated structures, whereas D-TPs in tannins showed increased unsaturation through higher DBE and AImod. In condensed aromatics, D-TPs displayed lower DBE, DBE-O, and AImod, along with higher O/C than D-free TPs. These findings align with previous research, highlighting the reactivity of unsaturated formulas and the transformation of saturated aromatic structures. Notably, saturated tannins exhibited higher reactivity due to their O/C ratio and lower aromaticity, allowing greater UV light absorption and generation of excited states.

III.3.3. Decoding UV-induced reactions via PMD-network analysis

The construction of a paired mass distance (PMD)-based network, guided by possible UV reactions, deciphered NOM transformations based on both structural categories and

molecular composition. For lignin/CRAMs and condensed aromatics, hydroxylation reactions with hydrogen substitution (+OD-H) dominated UV reactions. In contrast, tannins primarily exhibited nitro group loss (+D-NO_2). Molecular composition classification revealed hydroxylation as the dominant reaction observed UV reactions), with most reactions yielding D-TPs. Notably, the minor D-free TPs included decarboxylation (-CO_2), dehydration (-H_2O), and deformylation (-CH_2O).

Topological analysis of the PMD-network highlighted hubs with the highest degree, comprising either CHO or CHOS compounds. These hubs were mainly condensed aromatics and lignin/CRAMs, indicating a tendency for CHOS conversion to CHO compounds. Notably, CHOS and CHO formulas exhibited some commonalities in reactivity across different AOP treatments, aligning with observations from previous research. Correlations emerged between node degree, Gibbs energies for oxidation half-reactions (ΔG_{Cox}), and DBE/C. Hub nodes with degree eight shared common ΔG_{Cox} and DBE/C values, suggesting that hub formulas are more unsaturated and energetically favourable for transformation. TPs with higher O/C ratios displayed smaller ΔG_{Cox}, and increasing DBE corresponded to lower ΔG_{Cox}.

Structural changes revealed conversions from lignin-like to tannin formulas (mainly through hydroxylation and oxidative deamination), while deamination reactions were pivotal in transforming lignin-like to condensed aromatics. Conversely, tannins transformed into lignin and condensed aromatics, likely through nitro group loss. Some minor conversions between condensed aromatics and tannins also occurred, possibly due to OD group addition. Overall, these findings provide insights into complex NOM transformations under UV irradiation, revealing dominant reactions and structural shifts.

III.3.4. Deuterium isotope tracking analysis

Deuterium (D) was utilized as a stable isotope tracer to investigate reactivity towards OD radical reactions. Condensed aromatics and tannins displayed D-rich formulas, with several formulas containing up to 10 D atoms (referred to as 10th generation formulas). These 10th generation formulas were categorized into CHDO and CHDON. In the lignin/CRAM class, a maximum number of D atoms was observed. The 8th generation formula was affiliated with CHDONS, and formulas for the 7th generation were classified as CHDON. The high reactivity of condensed aromatics towards OH radical attack was attributed to their electron-rich structure, enabling sequential OH radical reactions through electron delocalization. Notably, a significant proportion of total CHDO and CHDON

formulas in condensed aromatics were associated with the 10th generation, indicating recalcitrant nitrogenous structures. The D isotope tracking analysis revealed parent formulas undergoing successive OD radical attacks with H-abstraction (+OD-H), resulting in distinct D-TPs found in the treated sample. Predicted structures for these formulas suggested that as the number of OD groups increased, lignin-like structures became more saturated, aligning with previous findings. The predicted structures also correlated with scavenger activity against OH radicals, highlighting the significance of specific functional groups and chemical features in lignin's structure. This approach holds potential for predicting TP structures and advancing the comprehension of mechanisms in UV treatment processes.

III.4. Conclusions

This study delved into the reactivity and transformation of NOM during UV irradiation. Analysing molecular compositions, CHOS type formulas exhibited the highest reactivity, while CHO formulas displayed the lowest reactivity. Tannins showed significant reactivity followed by condensed aromatics and lignin/CRAMs in terms of structural categories. Interpretable machine learning analysis identified MW, DBE-O, NOSC, and heteroatom presence (nitrogen and sulphur) as key factors governing formula reactivity, particularly larger and unsaturated NOM with S and N atoms. Specific molecular compositions within CHOS and CHO acted as hubs, influencing reactivity through multiple pathways. Paired mass difference network analysis highlighted hydroxylation reactions dominating UV reactions for lignin/CRAMs and condensed aromatics, resulting in more transformation products (TPs) than precursors. Certain TPs in condensed aromatics and tannins contained up to 10 D atoms, indicating successive reactions with OD radicals. These insights aid in identifying crucial reactive precursors and characterizing UV-induced TPs, though further research is needed to link TPs with functional aspects like biodegradability and biotoxicity.

III.5. Acknowledgements

This study is financially supported by JSPS Kakenhi (22H01623, 22KF0134)

CHAPTER IV Deciphering Lignin Reactivity and Transformations in UV Photolysis Studied by FT-ICR-MS and Interpretable Machine Learning

Related publication:

Dwinandha, D., Fu, QL., Elsamadony, M., Fujii, M. 2023. Deciphering Lignin Reactivity and Transformations in UV Photolysis Studied by FT-ICR-MS and Interpretable Machine Learning. (**Under preparation**)

IV.1. Introduction

Lignin, constituting a significant portion of plant biomass, has garnered interest in various industries for its potential applications. In water environments, it becomes part of soil organic matter and enters aquatic ecosystems as natural organic matter (NOM). NOM is a complex mixture with a crucial role in ultraviolet-based advanced oxidation processes (UV-AOPs). Understanding NOM reactivity and transformation is essential due to its impact on pollutant degradation efficiency, radical production inhibition, and the generation of transformation products. In this context, high-resolution mass spectrometry (HRMS) like Fourier transform ion cyclotron resonance mass spectrometry (FT-ICR-MS) has proven useful for molecular-level analysis. To address the complexity of NOM, investigating known structures like lignin can offer insights. Lignin's transformations under photo-irradiation have been documented, yet detailed mechanisms remain elusive.

Moreover, machine learning is gaining traction to describe NOM properties. Machine learning has revealed the relationship between NOM chemodiversity and microbial characteristics. However, its application to elucidate NOM reactivity during photooxidation remains scarce. Additionally, mass differences between molecules, as utilized in pairwise mass distance (PMD) analysis, offer valuable insights into organic matter transformations. Successfully employed for various treatments like UV exposure and anaerobic fermentation, PMD networks highlight key transformation reactions.

This study aims to investigate lignin's reactivity and transformations under UV exposure using FT-ICR-MS, interpretable machine learning, and PMD network analysis. By combining FT-ICR-MS with existing lignin structures, structural changes and functional group formations will be identified. Machine learning methods will correlate these alterations with physicochemical aspects. PMD networks will provide valuable information on transformation reactions. Ultimately, this research will enhance our understanding of lignin's behaviour during UV photolysis, contributing to insights into NOM's behaviour in UV-AOPs.

IV.2. Materials and Methods

IV.2.1. Materials and UV exposure experiment

Lignin alkali was obtained from Sigma-Aldrich and prepared at a concentration of 0.5 g/L, dissolved in 3 mL of water within a 5 mL quartz cell. UV exposure was conducted in a photoreactor with two 15-W UV lamps, and samples were collected after 48 and 72 hours, representing two stages of exposure, while a control sample remained in the dark. UV lamp intensity was 0.51 mW/cm², akin to typical water purification equipment settings.

Experiments were buffer-free to prevent potential buffer-derived radical formation. Post-experiment, 0.2 mL samples were diluted to 250 mL with ultrapure water and subjected to solid-phase extraction for dissolved organic matter (DOM). Acidification, gravitational passage through Bond Elut PPL cartridges, and methanol-based extraction were employed before FT-ICR MS measurement.

IV.2.2. FT-ICR MS analysis and formula assignment

The UV-treated and untreated samples were subjected to analysis using a 9.4T FT-ICR MS (Solarix XR, Bruker, Tohoku University). Electrospray ionization (ESI) in negative mode was employed, with a capillary voltage of -4.5 kV, injection rate of 150 μL/h, time domain data size of 2 M words, measurement m/z range spanning from 150 to 1500, and a resolution of approximately 200,000 (m/z = 399). Mass spectra were generated with 50 scan integrations, and peaks with an S/N ratio of 4 or higher were considered as signal peaks via DataAnalysis software (Bruker). For internal calibration, known CHO-homologous series of freshwater DOM (m/z = 200–600) were employed, ensuring mass accuracy (error < 1.0 ppm) with FT-ICR MS. The TRFu algorithm was used for molecular formula and molecular property identification. These parameters were subsequently weighted for each sample using specific equations. Furthermore, the calculation of Gibbs energies for oxidation half reactions of organic compounds was conducted according to established equations.

IV.2.3. Interpretable machine learning method

This study employs interpretable machine learning (XAI) for explanatory data analysis. XAI is chosen due to its superior predictive performance and ease of implementation compared to traditional models. The FT-ICR MS data collected from UV-exposed and untreated samples are compared across stages, with specific formulas labelled as "Disappeared" (reactive) or "Resistant" (unreactive) based on their presence. XGBoost, a gradient boosting model, is applied using 17 molecular properties as descriptors, and the model's behaviour is explained through post-hoc methods including feature importance, feature interaction, and partial dependence plots using SHAP. This approach provides insights into the contributions of molecular properties to reactivity.

IV.2.4. Mass difference and network analysis

Mass difference analysis involves linking parent and produced formulas to elucidate dominant reactions in the system. In each UV exposure stage, parent formulas from 0-hour

and 48-hour samples are connected to newly detected "produced" formulas, forming the basis for constructing a mass difference network. Transformation reactions are inferred from mass differences, although not all reactions are covered due to measurement limitations. Selected reactions encompass well-known UV-induced organic transformations. Gephi is utilized for network visualization and analysis, calculating node degrees and identifying hubs. While some reaction types are not considered, this approach effectively investigates transformation reactions in the UV-exposed system.

IV.3. Results and Discussion

IV.3.1. Overall characteristics of untreated and treated lignin after UV exposure

The number of formulas increased after 48-hour UV exposure and then decreased after 72 hours, indicating incomplete mineralization during the initial phase followed by further degradation. Formulas were categorized into different groups based on elemental composition, with CHO being the dominant molecular composition. Notably, the presence of sulphur (S) and phosphorus (P) in the lignin structure was also observed, potentially originating from various processes such as the Kraft process or geochemical interactions. Analysis of formulas in the untreated sample, after 48 hours, and after 72 hours of UV exposure revealed trends of increasing oxidation and decreasing saturation throughout the exposure period. The disappeared, resistant, and produced formulas were distinguished, with disappeared formulas interpreted as reactive and resistant formulas as unreactive. Formulas newly detected after exposure were labelled as "produced" formulas, representing products of reactions over time.

During the initial 48 hours, the "produced" formulas exhibited higher molecular weight and oxidation state but lower carbon number compared to disappeared or reactive formulas, indicating carbon chain loss and oxygen addition. Higher oxidation state signifies increased proportions of oxidized molecules due to the addition of electronegative atoms. Oxygen or oxygen group addition, likely in the form of carboxyl or hydroxyl groups, was a major contributor to increased oxidation and O/C ratios, consistent with previous studies. The presence of a significant carboxyl group formation was evidenced by the notable decrease in [DBE-O], indicating a higher number of carbon-oxygen double bonds. After 72 hours of irradiation, produced formulas showed increased molecular weight, oxidation, and [DBE-O], suggesting further oxidation and possible removal or mineralization of carboxyl-bearing formulas.

IV.3.2. Relationship between lignin molecular properties and its reactivity during UV exposure

Interpretable machine learning (XAI) provides valuable insights into lignin's reactivity through its molecular properties. By employing two models tailored to different stages of exposure, this approach effectively explains the underlying data trends. The models exhibit strong performance metrics (AUC = 0.99-0.99, accuracy = 0.96-0.97, sensitivity = 0.97-0.99, and specificity = 0.90-0.96), indicating their ability to elucidate the dataset. These models were interpreted using feature importance, partial dependence plots, and feature interactions.

The feature importance analysis reveals the distinctive influence of each molecular property on reactivity. In the initial stage of UV exposure, the presence of sulphur (nS) emerges as the most impactful factor, followed by molecular weight (MW), O/C ratio, AImod, and NOSC. In the subsequent stage, the order shifts to O/C, nC, MW, DBE/C, and NOSC. These findings underscore the central roles of molecular weight and O/C ratio in controlling lignin reactivity, consistent with the significance of MW and O/C in CHO-lignin-like structure groups observed in NOM mixtures. Furthermore, feature interactions analyses unveil the co-dependency between different features, with MW and O/C remaining crucial throughout the UV exposure, while elemental compositions (nO, nC, nH) gain prominence.

Interestingly, the shift in importance of sulphur-related features between the two stages is noteworthy. Although sulphur (nS) was highly influential in the initial stage, its impact diminished in the later stage, indicating the prominence of other functional groups during extended oxidation. Moreover, the 1D and 2D partial dependence plots shed light on the relationships between features and reactivity. For instance, high molecular weight and low oxygen contribution were correlated with increased reactivity. The study also suggests that reactive phenolic hydroxyl groups play a key role in the second stage, while sulfur's role diminishes over time, possibly due to oxidation into less reactive forms. Overall, these analyses offer a comprehensive understanding of lignin's reactivity, unveiling the intricate interplay between molecular properties and UV exposure.

IV.3.3. Tracking the possible key transformation reactions of lignin during UV photolysis

Key transformation reactions were explored using PMD networks based on potential UV-induced reactions. Gephi visualizations revealed dominant reactions during the 48-hour UV exposure: hydroxylation, accounting for the majority, followed by ketonization or quinone formation. These findings align with previous sections indicating oxygen group additions contributed to increased NOSC. Hydroxylation and ketone formation are known

main reactions in OH•-mediated processes. In the later stage, significant reactions involved carbon and hydrogen group losses, including dealkylation and deformylation. Aromatic ring oxidation and cleavage reactions leading to dicarboxylic acids formation were also likely.

The second stage exhibited fewer reactions than the first, possibly due to incomplete reaction coverage. In the first stage, CHO and CHOS formulas dominated nodes, while CHOP formulas gained prominence in the second stage. CHOS and CHOP were hubs in both stages, indicating high reactivity. Specifically, formulas $C_{18}H_{14}O_4S_1$, $C_7H_{13}O_7P_1$, and $C_{10}H_{17}O_8P_1$ were notable hubs. CHOP's reactivity highlights a novel avenue for exploring phosphorus-containing formula reactivity and its role in lignin oxidation.

IV.4. Conclusions

This study delved into lignin reactivity and transformation induced by UV exposure, employing FT ICR MS and interpretable machine learning. The analysis covered two stages of UV exposure: the initial 48 hours and up to 72 hours. Following 48 hours, a notable increase in formulas suggested incomplete mineralization of larger molecules, followed by further degradation. Lignin formulas exhibited increased oxidation and reduced saturation throughout UV exposure. Interpretable machine learning revealed molecular weight and oxygen-related properties as key factors influencing lignin reactivity, with nS impactful in the first stage but less so in the second, indicating the significance of other functional groups during extended oxidation. Aliphatic hydroxyl groups were prominent reactive sites initially, while phenolic hydroxyl groups gained reactivity in the later stage. Transformation reactions highlighted dominant hydroxylation and ketonization/quinone formation in the first stage, followed by dealkylation and deformylation in the later stage, suggesting aromatic ring oxidation and cleavage. In summary, this research offers insights into lignin transformation under UV exposure, shedding light on reactivity influencers and advancing our understanding of lignin's behaviour in various applications.

IV.5. Acknowledgements

This study is financially supported by JSPS Kakenhi.

CHAPTER V Conclusions and Recommendation

V.1. Conclusions

Advanced oxidation process (AOP) of organic pollutant does not yield in mineralization of the compounds, instead it forms transformation products which possess potential risks to human and environmental health. This study aimed to elucidate the transformation products of organic compounds during •OH-based AOP by applying in silico and experimental method with two specific objectives.

First, investigation of the feasibility of theoretical approach using quantum chemical calculation as an alternative for assessing the transformation products of organic compounds during AOP. The feasibility was measured based on accuracy and calculation cost. Assessment for phenol and its major TPs resulting in good accuracy for calculating molecular structures and reaction sites, which were obtained with high level of theory (M062X). However, calculation of reaction rate constant was still produced a considerable gap compared to experimentally calculated rate constant. The error can be attributed to the limitation of current method which does not consider dispersion effect and multireference character in the calculated system. Moreover, the calculation time took more than 72 hours for one molecule using a workstation (Intel Xeon/2.1 GHz/RAM 128GB). Thus, strategies for improvement including minimizing the error and calculation time are still needed for QCC to serve as an alternative assessment method.

Second objective was combining experimental (FT-ICR-MS) and in silico (as post-experimental analysis to assess the transformations of naturally-occurring organic matter during AOP. There are two cases for this objective: natural organic matter (NOM) and lignin photolysis. For NOM, the experiment was conducted for 12 hours irradiation time. According to the analyses based on the molecular composition, CHOS formulas shows higher reactivity followed by CHON and CHO formulas, whereas in terms of structural category, the order of reactivity was tannins > condensed aromatics > lignin/CRAMs. Analyses of the reactive and unreactive formulas using interpretable machine learning approach revealed that overall MW, DBE-O, NOSC and presence of heteroatoms are the crucial features regulating the formula reactivity, and such larger-size and unsaturated NOM containing S and N atoms tended to be reactive against the UV irradiation. The paired mass difference network analyses further indicated that

hydroxylation reactions dominated the UV reactions for lignin/CRAMs and condensed aromatics.

In case of lignin, 48-h and 72-h irradiated lignin was observed. After 48 hours of exposure, the number of formulas increased significantly, suggesting incomplete mineralization of larger molecules to smaller ones. This was followed by further degradation of the smaller molecules after 72 hours. The lignin formulas were found to be more oxidized and less saturated throughout the UV exposure. Using interpretable machine learning, it was found that molecular weight and properties related to oxygen and oxidation state (nO, O/C, and NOSC) were the most influential molecular properties in determining lignin reactivity. Furthermore, aliphatic hydroxyl groups were suggested as major reactive functional groups in the first stage of UV exposure, while in the second stage phenolic hydroxyl groups was the most reactive. Key transformation reactions of lignin during UV photolysis were investigated, with hydroxylation and ketonization/quinone formation being dominant in the first stage. Dealkylation and deformylation reactions were observed in the later stage, suggesting the occurrence of aromatic ring oxidation and cleavage.

V.2. Implications to environment and society

This study provides insight into transformation product formation mechanisms using in silico (quantum chemical calculation as theoretical approach and interpretable machine learning as computational approach) in combination with experimental approach (FT-ICR MS). In the first study, procedures to predict, calculate, and analysed TP formation from a certain compounds were developed and presented, allowing the understanding of compound behaviour, reactivity, and potential degradation pathways. Extended analysis of this study will lead to producing a full transformation network with the reaction characteristics of pollutants in water. Similar strategy could be implemented for different chemicals or pollutants by replacing the observed molecular structure, suggesting its application to a diverse range of pollutants. However, the most crucial challenges for full implementation revolves around computational resources and expertise, such as the computational complexity, modelling the realistic environmental systems, validation and benchmarking to ensure the reliability, and accessibility and educational requirement to advanced computational tools especially for researches in

developing regions. In addition, the needs of experimental validation will persist even if the computational resources and expertise limitations perish. The nature of theoretical approach itself is predicting environmental processes using computation or numerical methods from fundamental principles and equations, as opposed to experimental methods which emphasize real-world interactions and direct measurement of a phenomena. Therefore, the integration of theoretical and experimental approaches holds immense promise for advancing scientific understanding and it is unlikely that either approach will entirely replace the other. The synergy between theoretical models and empirical data allows for a more comprehensive comprehension of complex environmental processes. The research underscores the significance of employing both approaches to enhance predictive accuracy and refine hypotheses, thereby leading to more informed decisions.

Second and third study attempted to explore and breakdown the implicit information that implying the transformation occurred in organic matter from FT-ICR MS data using interpretable machine learning method and network analysis. As the current research progresses in non-target screening using high resolution mass spectrometry (HRMS), post-analysis tools are being significantly developed to interpret the results. This study offers an accessible and simplistic procedures as exploratory data analysis connected to the expected reaction mechanisms for transformation product assessment. Furthermore, some interesting results were obtained, for example the relevance of nitrogen and sulphur in determining the organic matter reactivity, which generally derived from biomolecule from microbial metabolism, suggesting the importance of biological treatment before UV irradiation to degrade some of the organic molecules. Nevertheless, the study's intention for characterizing and identifying the transformation mechanisms is still in the lab stage and should be followed by further research regarding its practical implementation based on the produced knowledge. The practical information hopefully will assist the consideration in policy-making regarding the transformation product and advanced oxidation process.

V.3. Limitations and recommendations

The current research poses several limitations, which are described as follows:

- The theoretical framework in the Chapter 2 was developed with an intention as an initial TP assessment for any selected organic pollutants in each case study. However, only one model compound was used and three level of theory with a certain basis set and implicit solvation. Furthermore, the interactions between each molecules were only represented by Fukui values, activation energy, and kinetic rate constant. All this simplified calculation settings might be insufficient to capture the actual reaction behaviour in real water sample due to the complexity of the actual water matrix itself.
- In Chapter 3 and 4, the study might have focused on a specific natural organic matter sample or a narrow range of environmental conditions during UV photolysis. As a result, the findings might not be directly applicable to other types of natural organic matter or different photolysis conditions, limiting the generalizability of the results.
- Interpretable machine learning models used in the study may be subject to potential biases in the training data, feature selection, or model assumptions. These biases could impact the accuracy and interpretation of the machine learning predictions, potentially leading to oversimplified or misleading insights into the reactivity and transformation processes of natural organic matter during UV photolysis.
- UV photolysis is just one of many processes that natural organic matter may undergo in environmental systems. Isolating the specific effects of UV photolysis from other concurrent environmental factors, such as microbial degradation or redox reactions, can be challenging. The study might face difficulties in definitively attributing observed changes in natural organic matter solely to UV photolysis.

The recommendations for future studies are summarized as follows:

- Further investigation using a set range of chemicals from smallest to largest with more basis sets and different solvation condition could be beneficial to further understand the limit of QCC for alternative approach.

- For the NOM and lignin transformations and reactivity during UV photolysis, elucidation of structural changes is still a major challenge because there are a lot of missing information by not having structure of the compounds. Thus, future studies that focused on the strategy to obtain structures is needed to connect the reactivity, type of reaction occurs, and the reaction product.

BIBLIOGRAPHY

(1) Alsbaiee, A.; Smith, B. J.; Xiao, L.; Ling, Y.; Helbling, D. E.; Dichtel, W. R. Rapid Removal of Organic Micropollutants from Water by a Porous β-Cyclodextrin Polymer. *Nature* **2016**, *529* (7585), 190–194. https://doi.org/10.1038/nature16185.

(2) Richardson, S. D.; Ternes, T. A. Water Analysis: Emerging Contaminants and Current Issues. *Anal. Chem.* **2018**, *90* (1), 398–428. https://doi.org/10.1021/acs.analchem.7b04577.

(3) Schwarzenbach, R. P.; Escher, B. I.; Fenner, K.; Hofstetter, T. B.; Johnson, C. A.; von Gunten, U.; Wehrli, B. The Challenge of Micropollutants in Aquatic Systems. **2006**, No. August, 1072–1078.

(4) Wang, W.; Chen, M.; Wang, D.; Yan, M.; Liu, Z. Different Activation Methods in Sulfate Radical-Based Oxidation for Organic Pollutants Degradation: Catalytic Mechanism and Toxicity Assessment of Degradation Intermediates. *Sci. Total Environ.* **2021**, *772*, 145522. https://doi.org/10.1016/j.scitotenv.2021.145522.

(5) Pai, C. W.; Wang, G. S. Treatment of PPCPs and Disinfection By-Product Formation in Drinking Water through Advanced Oxidation Processes: Comparison of UV, UV/Chlorine, and UV/H2O2. *Chemosphere* **2022**, *287* (P3), 132171. https://doi.org/10.1016/j.chemosphere.2021.132171.

(6) Liu, X.; Zhang, T.; Zhou, Y.; Fang, L.; Shao, Y. Degradation of Atenolol by UV/Peroxymonosulfate: Kinetics, Effect of Operational Parameters and Mechanism. *Chemosphere* **2013**, *93* (11), 2717–2724. https://doi.org/10.1016/j.chemosphere.2013.08.090.

(7) Monteagudo, J. M.; El-taliawy, H.; Durán, A.; Caro, G.; Bester, K. Sono-Activated Persulfate Oxidation of Diclofenac : Degradation , Kinetics , Pathway and Contribution of the Di Ff Erent Radicals Involved. *J. Hazard. Mater.* **2018**, *357* (April), 457–465. https://doi.org/10.1016/j.jhazmat.2018.06.031.

(8) Bourgin, M.; Beck, B.; Boehler, M.; Borowska, E.; Fleiner, J.; Salhi, E.; Teichler, R.; von Gunten, U.; Siegrist, H.; McArdell, C. S. Evaluation of a Full-Scale Wastewater Treatment Plant Upgraded with Ozonation and Biological Post-

Treatments: Abatement of Micropollutants, Formation of Transformation Products and Oxidation by-Products. *Water Res.* **2018**, *129*, 486–498. https://doi.org/10.1016/j.watres.2017.10.036.

(9) Wardenier, N.; Liu, Z.; Nikiforov, A.; Van Hulle, S. W. H.; Leys, C. Micropollutant Elimination by O3, UV and Plasma-Based AOPs: An Evaluation of Treatment and Energy Costs. *Chemosphere* **2019**. https://doi.org/10.1016/j.chemosphere.2019.06.033.

(10) Gomes Júnior, O.; Batista, L. L.; Ueira-Vieira, C.; Sousa, R. M. F.; Starling, M. C. V. M.; Trovó, A. G. Degradation Mechanism of Fipronil and Its Transformation Products, Matrix Effects and Toxicity during the Solar/Photo-Fenton Process Using Ferric Citrate Complex. *J. Environ. Manage.* **2020**, *269* (May). https://doi.org/10.1016/j.jenvman.2020.110756.

(11) Gümüş, D.; Akbal, F. Comparison of Fenton and Electro-Fenton Processes for Oxidation of Phenol. *Process Saf. Environ. Prot.* **2016**, *103* (3), 252–258. https://doi.org/10.1016/j.psep.2016.07.008.

(12) Diak, M.; Klein, M.; Klimczuk, T.; Lisowski, W.; Remita, H.; Zaleska-Medynska, A.; Grabowska, E. Photoactivity of Decahedral TiO2 Loaded with Bimetallic Nanoparticles: Degradation Pathway of Phenol-1-13C and Hydroxyl Radical Formation. *Appl. Catal. B Environ.* **2017**, *200*, 56–71. https://doi.org/10.1016/j.apcatb.2016.06.067.

(13) Gao, Y. qiong; Zhang, J.; Li, C.; Tian, F. xiang; Gao, N. yun. Comparative Evaluation of Metoprolol Degradation by UV/Chlorine and UV/H2O2 Processes. *Chemosphere* **2020**, *243*, 125325. https://doi.org/10.1016/j.chemosphere.2019.125325.

(14) von Gunten, U. Oxidation Processes in Water Treatment: Are We on Track? *Environ. Sci. Technol.* **2018**, *52* (9), 5062–5075. https://doi.org/10.1021/acs.est.8b00586.

(15) Wang, C.; Moore, N.; Bircher, K.; Andrews, S.; Hofmann, R. Full-Scale Comparison of UV/H2O2 and UV/Cl2 Advanced Oxidation: The Degradation of Micropollutant Surrogates and the Formation of Disinfection Byproducts. *Water Res.* **2019**, *161*, 448–458. https://doi.org/10.1016/j.watres.2019.06.033.

(16) Gottschalk, C.; Libra, J.; Saupe, A. Ozone in Overview. *Ozonation water waste*

water a Pract. Guid. to Underst. ozone its Appl. Wiley-Vch., Weinheim, Ger. **2000**, 5–35.

(17) Kim, I.; Yamashita, N.; Tanaka, H. Performance of UV and UV/H2O2 Processes for the Removal of Pharmaceuticals Detected in Secondary Effluent of a Sewage Treatment Plant in Japan. *J. Hazard. Mater.* **2009**, *166* (2–3), 1134–1140. https://doi.org/10.1016/j.jhazmat.2008.12.020.

(18) Feng, S.; Zhang, X.; Liu, Y. New Insights into the Primary Phototransformation of Acetaminophen by UV/H2O2: Photo-Fries Rearrangement versus Hydroxyl Radical Induced Hydroxylation. *Water Res.* **2015**, *86*, 35–45. https://doi.org/10.1016/j.watres.2015.05.008.

(19) Kim, T.; Don, S.; Young, H.; Joo, S.; Lee, M.; Yu, S. Degradation and Toxicity Assessment of Sulfamethoxazole and Chlortetracycline Using Electron Beam , Ozone and UV. *J. Hazard. Mater.* **2012**, *227–228*, 237–242. https://doi.org/10.1016/j.jhazmat.2012.05.038.

(20) Yu, H. W.; Anumol, T.; Park, M.; Pepper, I.; Scheideler, J.; Snyder, S. A. On-Line Sensor Monitoring for Chemical Contaminant Attenuation during UV/H2O2 Advanced Oxidation Process. *Water Res.* **2015**, *81*, 250–260. https://doi.org/10.1016/j.watres.2015.05.064.

(21) Wols, B. A.; Hofman-Caris, C. H. M.; Harmsen, D. J. H.; Beerendonk, E. F. Degradation of 40 Selected Pharmaceuticals by UV/H2O2. *Water Res.* **2013**, *47* (15), 5876–5888. https://doi.org/10.1016/j.watres.2013.07.008.

(22) Lajeunesse, A.; Gagnon, C.; Sauvé, S. Determination of Basic Antidepressants and Their N-Desmethyl Metabolites in Raw Sewage and Wastewater Using Solid-Phase Extraction and Liquid Chromatography-Tandem Mass Spectrometry. *Anal. Chem.* **2008**, *80* (14), 5325–5333. https://doi.org/10.1021/ac800162q.

(23) Larsson, E.; Jönsson, J. Å. Science of the Total Environment Behaviour of Nonsteroidal Anti-in Fl Ammatory Drugs and Eight of Their Metabolites during Wastewater Treatment Studied by Hollow Fi Bre Liquid Phase Microextraction and Liquid Chromatography Mass Spectrometry. *Sci. Total Environ.* **2014**, *485–486*, 300–308. https://doi.org/10.1016/j.scitotenv.2014.03.055.

(24) Miao, X. S.; Metcalfe, C. D. Determination of Carbamazepine and Its Metabolites in Aqueous Samples Using Liquid Chromatography - Electrospray

Tandem Mass Spectrometry. *Anal. Chem.* **2003**, *75* (15), 3731–3738. https://doi.org/10.1021/ac030082k.

(25) Rubirola, A.; Llorca, M.; Rodriguez-Mozaz, S.; Casas, N.; Rodriguez-Roda, I.; Barceló, D.; Buttiglieri, G. Characterization of Metoprolol Biodegradation and Its Transformation Products Generated in Activated Sludge Batch Experiments and in Full Scale WWTPs. *Water Res.* **2014**, *63*, 21–32. https://doi.org/10.1016/j.watres.2014.05.031.

(26) Subedi, B.; Kannan, K. Occurrence and Fate of Select Psychoactive Pharmaceuticals and Antihypertensives in Two Wastewater Treatment Plants in New York State, USA. *Sci. Total Environ.* **2015**, *514*, 273–280. https://doi.org/10.1016/j.scitotenv.2015.01.098.

(27) Zuehlke, S.; Duennbier, U.; Heberer, T. Investigation of the Behavior and Metabolism of Pharmaceutical Residues during Purification of Contaminated Ground Water Used for Drinking Water Supply. *Chemosphere* **2007**, *69* (11), 1673–1680. https://doi.org/10.1016/j.chemosphere.2007.06.020.

(28) Osorio, V.; Imbert-Bouchard, M.; Zonja, B.; Abad, J. L.; Pérez, S.; Barceló, D. Simultaneous Determination of Diclofenac, Its Human Metabolites and Microbial Nitration/Nitrosation Transformation Products in Wastewaters by Liquid Chromatography/Quadrupole-Linear Ion Trap Mass Spectrometry. *J. Chromatogr. A* **2014**, *1347*, 63–71. https://doi.org/10.1016/j.chroma.2014.04.058.

(29) Freeling, F.; Alygizakis, N. A.; von der Ohe, P. C.; Slobodnik, J.; Oswald, P.; Aalizadeh, R.; Cirka, L.; Thomaidis, N. S.; Scheurer, M. Occurrence and Potential Environmental Risk of Surfactants and Their Transformation Products Discharged by Wastewater Treatment Plants. *Sci. Total Environ.* **2019**, *681*, 475–487. https://doi.org/10.1016/j.scitotenv.2019.04.445.

(30) Olak-Kucharczyk, M.; Ledakowicz, S. Advanced Oxidation of Preservative Agents in H2O2/UVC System – Kinetics Study, Transformation Products and Toxicity Assessment. *J. Hazard. Mater.* **2017**, *333*, 348–357. https://doi.org/10.1016/j.jhazmat.2017.03.047.

(31) Legrini, O.; Oliveros, E.; Braun, A. M. Photochemical Processes for Water Treatment. *Chem. Rev.* **1993**, *93* (2), 671–698. https://doi.org/10.1021/cr00018a003.

(32) Alnaizy, R.; Akgerman, A. Advanced Oxidation of Phenolic Compounds. *Adv. Environ. Res.* **2000**, *4* (3), 233–244. https://doi.org/10.1016/S1093-0191(00)00024-1.

(33) Lekkerkerker-Teunissen, K.; Benotti, M. J.; Snyder, S. A.; Van Dijk, H. C. Transformation of Atrazine, Carbamazepine, Diclofenac and Sulfamethoxazole by Low and Medium Pressure UV and UV/H2O2 Treatment. *Sep. Purif. Technol.* **2012**, *96*, 33–43. https://doi.org/10.1016/j.seppur.2012.04.018.

(34) Jallouli, N.; Elghniji, K.; Hentati, O.; Ribeiro, A. R.; Silva, A. M. T.; Ksibi, M. UV and Solar Photo-Degradation of Naproxen: TiO2 Catalyst Effect, Reaction Kinetics, Products Identification and Toxicity Assessment. *J. Hazard. Mater.* **2016**, *304*, 329–336. https://doi.org/10.1016/j.jhazmat.2015.10.045.

(35) Semitsoglou-Tsiapou, S.; Templeton, M. R.; Graham, N. J. D.; Hernández Leal, L.; Martijn, B. J.; Royce, A.; Kruithof, J. C. Low Pressure UV/H2O2 Treatment for the Degradation of the Pesticides Metaldehyde, Clopyralid and Mecoprop - Kinetics and Reaction Product Formation. *Water Res.* **2016**, *91*, 285–294. https://doi.org/10.1016/j.watres.2016.01.017.

(36) Lai, W. W. P.; Hsu, M. H.; Lin, A. Y. C. The Role of Bicarbonate Anions in Methotrexate Degradation via UV/TiO2: Mechanisms, Reactivity and Increased Toxicity. *Water Res.* **2017**, *112*, 157–166. https://doi.org/10.1016/j.watres.2017.01.040.

(37) Wols, B. A.; Harmsen, D. J. H.; Beerendonk, E. F.; Hofman-Caris, C. H. M. Predicting Pharmaceutical Degradation by UV (MP)/H2O2 Processes: A Kinetic Model. *Chem. Eng. J.* **2015**, *263*, 336–345. https://doi.org/10.1016/j.cej.2014.10.101.

(38) Li, Y.; Song, W.; Fu, W.; Tsang, D. C. W.; Yang, X. The Roles of Halides in the Acetaminophen Degradation by UV/H2O2 Treatment: Kinetics, Mechanisms, and Products Analysis. *Chem. Eng. J.* **2015**, *271*, 214–222. https://doi.org/10.1016/j.cej.2015.02.090.

(39) Khan, I. A.; Lee, Y. S.; Kim, J. O. Chemically Enhanced Pretreatment (CEPT) to Reduce Irreversible Fouling during the Clean-in-Place Process for Membranes Operating under Constant Flux and Constant Pressure Filtration. *Desalination* **2023**, *549* (September 2022), 116313.

https://doi.org/10.1016/j.desal.2022.116313.

(40) Wang, W. L.; Wu, Q. Y.; Du, Y.; Huang, N.; Hu, H. Y. Elimination of Chlorine-Refractory Carbamazepine by Breakpoint Chlorination: Reactive Species and Oxidation Byproducts. *Water Res.* **2018**, *129*, 115–122. https://doi.org/10.1016/j.watres.2017.11.016.

(41) Prasse, C.; Stalter, D.; Schulte-Oehlmann, U.; Oehlmann, J.; Ternes, T. A. Spoilt for Choice: A Critical Review on the Chemical and Biological Assessment of Current Wastewater Treatment Technologies. *Water Res.* **2015**, *87*, 237–270. https://doi.org/10.1016/j.watres.2015.09.023.

(42) Haddad, T.; Baginska, E.; Kümmerer, K. *Transformation Products of Antibiotic and Cytostatic Drugs in the Aquatic Cycle That Result from Effluent Treatment and Abiotic/Biotic Reactions in the Environment: An Increasing Challenge Calling for Higher Emphasis on Measures at the Beginning of the Pi*; 2015; Vol. 72. https://doi.org/10.1016/j.watres.2014.12.042.

(43) Wang, W.-L. L.; Wu, Q.-Y. Y.; Huang, N.; Xu, Z.-B. Bin; Lee, M.-Y. Y.; Hu, H.-Y. Y.; Huang, N.; Wu, Q.-Y. Y. Potential Risks from UV/H2O2 Oxidation and UV Photocatalysis: A Review of Toxic, Assimilable, and Sensory-Unpleasant Transformation Products. *Water Res.* **2018**, *141*, 109–125. https://doi.org/10.1016/j.watres.2018.05.005.

(44) Hofman-Caris, R. C. H. M.; Harmsen, D. J. H.; Puijker, L.; Baken, K. A.; Wols, B. A.; Beerendonk, E. F.; Keltjens, L. L. M. Influence of Process Conditions and Water Quality on the Formation of Mutagenic Byproducts in UV/H2O2 Processes. *Water Res.* **2015**, *74*, 191–202. https://doi.org/10.1016/j.watres.2015.01.035.

(45) Stalter, D.; Magdeburg, A.; Oehlmann, J. Comparative Toxicity Assessment of Ozone and Activated Carbon Treated Sewage Effluents Using an in Vivo Test Battery. *Water Res.* **2010**, *44* (8), 2610–2620. https://doi.org/10.1016/j.watres.2010.01.023.

(46) Cao, N.; Yang, M.; Zhang, Y.; Hu, J.; Ike, M.; Hirotsuji, J.; Matsui, H.; Inoue, D.; Sei, K. Evaluation of Wastewater Reclamation Technologies Based on in Vitro and in Vivo Bioassays. *Sci. Total Environ.* **2009**, *407* (5), 1588–1597. https://doi.org/10.1016/j.scitotenv.2008.10.048.

(47) Coelho, A. D.; Sans, C.; Agüera, A.; Gómez, M. J.; Esplugas, S.; Dezotti, M. Effects of Ozone Pre-Treatment on Diclofenac: Intermediates, Biodegradability and Toxicity Assessment. *Sci. Total Environ.* **2009**, *407* (11), 3572–3578. https://doi.org/10.1016/j.scitotenv.2009.01.013.

(48) Lester, Y.; Mamane, H.; Zucker, I.; Avisar, D. Treating Wastewater from a Pharmaceutical Formulation Facility by Biological Process and Ozone. *Water Res.* **2013**, *47* (13), 4349–4356. https://doi.org/10.1016/j.watres.2013.04.059.

(49) Li, G. Q.; Yu, T.; Wu, Q. Y.; Lu, Y.; Hu, H. Y. Development of an ATP Luminescence-Based Method for Assimilable Organic Carbon Determination in Reclaimed Water. *Water Res.* **2017**, *123*, 345–352. https://doi.org/10.1016/j.watres.2017.06.082.

(50) Antonopoulou, M.; Evgenidou, E.; Lambropoulou, D.; Konstantinou, I. A Review on Advanced Oxidation Processes for the Removal of Taste and Odor Compounds from Aqueous Media. *Water Res.* **2014**, *53*, 215–234. https://doi.org/10.1016/j.watres.2014.01.028.

(51) Lambropoulou, D.; Evgenidou, E.; Saliverou, V.; Kosma, C.; Konstantinou, I. Degradation of Venlafaxine Using TiO2/UV Process: Kinetic Studies, RSM Optimization, Identification of Transformation Products and Toxicity Evaluation. *J. Hazard. Mater.* **2017**, *323*, 513–526. https://doi.org/10.1016/j.jhazmat.2016.04.074.

(52) Antonopoulou, M.; Hela, D.; Konstantinou, I. Photocatalytic Degradation Kinetics, Mechanism and Ecotoxicity Assessment of Tramadol Metabolites in Aqueous TiO2 Suspensions. *Sci. Total Environ.* **2016**, *545–546*, 476–485. https://doi.org/10.1016/j.scitotenv.2015.12.088.

(53) Choi, H. J.; Kim, D.; Lee, T. J. Photochemical Degradation of Atrazine in UV and UV/H2O2 Process: Pathways and Toxic Effects of Products. *J. Environ. Sci. Heal. - Part B Pestic. Food Contam. Agric. Wastes* **2013**, *48* (11), 927–934. https://doi.org/10.1080/03601234.2013.816587.

(54) Herrmann, M.; Menz, J.; Olsson, O.; Kümmerer, K. Identification of Phototransformation Products of the Antiepileptic Drug Gabapentin: Biodegradability and Initial Assessment of Toxicity. *Water Res.* **2015**, *85*, 11–21. https://doi.org/10.1016/j.watres.2015.08.004.

(55) Solís, R. R.; Rivas, F. J.; Martínez-Piernas, A.; Agüera, A. Ozonation, Photocatalysis and Photocatalytic Ozonation of Diuron: Intermediates Identification. *Chem. Eng. J.* **2016**, *292*, 72–81. https://doi.org/10.1016/j.cej.2016.02.005.

(56) Donner, E.; Kosjek, T.; Qualmann, S.; Kusk, K. O.; Heath, E.; Revitt, D. M.; Ledin, A.; Andersen, H. R. Ecotoxicity of Carbamazepine and Its UV Photolysis Transformation Products. *Sci. Total Environ.* **2013**, *443*, 870–876. https://doi.org/10.1016/j.scitotenv.2012.11.059.

(57) Michael, I.; Achilleos, A.; Lambropoulou, D.; Torrens, V. O.; Pérez, S.; Petrović, M.; Barceló, D.; Fatta-Kassinos, D. Proposed Transformation Pathway and Evolution Profile of Diclofenac and Ibuprofen Transformation Products during (Sono)Photocatalysis. *Appl. Catal. B Environ.* **2014**, *147*, 1015–1027. https://doi.org/10.1016/j.apcatb.2013.10.035.

(58) Zhao, Y.; Yu, G.; Chen, S.; Zhang, S.; Wang, B.; Huang, J.; Deng, S.; Wang, Y. Ozonation of Antidepressant Fluoxetine and Its Metabolite Product Norfluoxetine: Kinetics, Intermediates and Toxicity. *Chem. Eng. J.* **2017**, *316*, 951–963. https://doi.org/10.1016/j.cej.2017.02.032.

(59) Li, A. J.; Schmitz, O. J.; Stephan, S.; Lenzen, C.; Yue, P. Y.-K.; Li, KaibinLi, H.; Leung, K. S.-Y. Photocatalytic Transformation of Acesulfame: Transformation Products Identification and Embryotoxicity Study. *Water Res.* **2016**, *89*, 68–75. https://doi.org/10.1016/j.watres.2015.11.035.

(60) García-Galán, M. J.; Anfruns, A.; Gonzalez-Olmos, R.; Rodriguez-Mozaz, S.; Comas, J. Advanced Oxidation of the Antibiotic Sulfapyridine by UV/H2O2: Characterization of Its Transformation Products and Ecotoxicological Implications. *Chemosphere* **2016**, *147*, 451–459. https://doi.org/10.1016/j.chemosphere.2015.12.108.

(61) Jimenez-Villarin, J.; Serra-Clusellas, A.; Martínez, C.; Conesa, A.; Garcia-Montaño, J.; Moyano, E. Liquid Chromatography Coupled to Tandem and High Resolution Mass Spectrometry for the Characterisation of Ofloxacin Transformation Products after Titanium Dioxide Photocatalysis. *J. Chromatogr. A* **2016**, *1443*, 201–210. https://doi.org/10.1016/j.chroma.2016.03.063.

(62) Roscher, J.; Vogel, M.; Karst, U. Identification of Ultraviolet Transformation

Products of Diclofenac by Means of Liquid Chromatography and Mass Spectrometry. *J. Chromatogr. A* **2016**, *1457*, 59–65. https://doi.org/10.1016/j.chroma.2016.06.027.

(63) González-Mariño, I.; Rodríguez, I.; Rojo, L.; Cela, R. Photodegradation of Nitenpyram under UV and Solar Radiation: Kinetics, Transformation Products Identification and Toxicity Prediction. *Sci. Total Environ.* **2018**, *644*, 995–1005. https://doi.org/10.1016/j.scitotenv.2018.06.318.

(64) Seiwert, B.; Golan-Rozen, N.; Weidauer, C.; Riemenschneider, C.; Chefetz, B.; Hadar, Y.; Reemtsma, T. Electrochemistry Combined with LC-HRMS: Elucidating Transformation Products of the Recalcitrant Pharmaceutical Compound Carbamazepine Generated by the White-Rot Fungus Pleurotus Ostreatus. *Environ. Sci. Technol.* **2015**, *49* (20), 12342–12350. https://doi.org/10.1021/acs.est.5b02229.

(65) Li, S.; Hu, J. Transformation Products Formation of Ciprofloxacin in UVA/LED and UVA/LED/TiO2systems: Impact of Natural Organic Matter Characteristics. *Water Res.* **2018**, *132*, 320–330. https://doi.org/10.1016/j.watres.2017.12.065.

(66) Menacherry, S. P. M.; Aravind, U. K.; Aravindakumar, C. T. Critical Review on the Role of Mass Spectrometry in the AOP Based Degradation of Contaminants of Emerging Concern (CECs) in Water. *J. Environ. Chem. Eng.* **2022**, *10* (4), 108155. https://doi.org/10.1016/j.jece.2022.108155.

(67) Menacherry, S. P. M.; Kočárek, M.; Kacerova, T.; Kotíková, Z.; Kačer, P.; Kodešová, R. The Impact of Initial Concentration of Selected Pharmaceuticals on Their Early Stage of Dissipation in Soils. *J. Soils Sediments* **2022**, *22* (2), 522–535. https://doi.org/10.1007/s11368-021-03095-7.

(68) Hermosilla, D.; Han, C.; Nadagouda, M. N.; Machala, L.; Gascó, A.; Campo, P.; Dionysiou, D. D. Environmentally Friendly Synthesized and Magnetically Recoverable Designed Ferrite Photo-Catalysts for Wastewater Treatment Applications. *J. Hazard. Mater.* **2020**, *381* (April 2019), 121200. https://doi.org/10.1016/j.jhazmat.2019.121200.

(69) Ioannou-Ttofa, L.; Raj, S.; Prakash, H.; Fatta-Kassinos, D. Solar Photo-Fenton Oxidation for the Removal of Ampicillin, Total Cultivable and Resistant E. Coli and Ecotoxicity from Secondary-Treated Wastewater Effluents. *Chem. Eng. J.*

2019, *355* (May 2018), 91–102. https://doi.org/10.1016/j.cej.2018.08.057.

(70) Klampfl, C. W. Metabolization of Pharmaceuticals by Plants after Uptake from Water and Soil: A Review. *TrAC - Trends Anal. Chem.* **2019**, *111*, 13–26. https://doi.org/10.1016/j.trac.2018.11.042.

(71) Li, J.; Jiang, J.; Pang, S.; Zhou, Y.; Gao, Y.; Yang, Y.; Sun, S.; Liu, G.; Ma, J.; Jiang, C.; Wang, L. Transformation of Methylparaben by Aqueous Permanganate in the Presence of Iodide: Kinetics, Modeling, and Formation of Iodinated Aromatic Products. *Water Res.* **2018**, *135*, 75–84. https://doi.org/10.1016/j.watres.2018.02.014.

(72) Parry, E.; Young, T. M. Comparing Targeted and Non-Targeted High-Resolution Mass Spectrometric Approaches for Assessing Advanced Oxidation Reactor Performance. *Water Res.* **2016**, *104*, 72–81. https://doi.org/10.1016/j.watres.2016.07.056.

(73) Guo, Z.; Huang, S.; Wang, J.; Feng, Y. L. Recent Advances in Non-Targeted Screening Analysis Using Liquid Chromatography - High Resolution Mass Spectrometry to Explore New Biomarkers for Human Exposure. *Talanta* **2020**, *219* (May), 121339. https://doi.org/10.1016/j.talanta.2020.121339.

(74) Xiao, R.; Gao, L.; Wei, Z.; Spinney, R.; Luo, S.; Wang, D.; Dionysiou, D. D.; Tang, C. J.; Yang, W. Mechanistic Insight into Degradation of Endocrine Disrupting Chemical by Hydroxyl Radical: An Experimental and Theoretical Approach. *Environ. Pollut.* **2017**, *231*, 1446–1452. https://doi.org/10.1016/j.envpol.2017.09.006.

(75) Tentscher, P. R.; Bourgin, M.; Von Gunten, U. Ozonation of Para -Substituted Phenolic Compounds Yields p -Benzoquinones, Other Cyclic α,β-Unsaturated Ketones, and Substituted Catechols. *Environ. Sci. Technol.* **2018**, *52* (8), 4763–4773. https://doi.org/10.1021/acs.est.8b00011.

(76) Kamath, D.; Mezyk, S. P.; Minakata, D. Elucidating the Elementary Reaction Pathways and Kinetics of Hydroxyl Radical-Induced Acetone Degradation in Aqueous Phase Advanced Oxidation Processes. *Environ. Sci. Technol.* **2018**, *52* (14), 7763–7774. https://doi.org/10.1021/acs.est.8b00582.

(77) Xiao, R.; Noerpel, M.; Ling Luk, H.; Wei, Z.; Spinney, R. Thermodynamic and Kinetic Study of Ibuprofen with Hydroxyl Radical: A Density Functional Theory

Approach. *Int. J. Quantum Chem.* **2014**, *114* (1), 74–83. https://doi.org/10.1002/qua.24518.

(78) Huerta-Fontela, M.; Galceran, M. T.; Ventura, F. Ultraperformance Liquid Chromatography Tandem Mass Spectrometry Analysis of Stimulatory Drugs of Abuse in Wastewater and Surface Waters. *Anal. Chem.* **2007**, *79* (10), 3821–3829. https://doi.org/10.1021/ac062370x.

(79) Terzi, S.; Senta, I.; Ahel, M.; Gros, M.; Petrovi, M.; Barcelo, D.; Müller, J.; Knepper, T.; Martí, I.; Ventura, F.; Jovan, P.; Jabu, D.; Terzić, S.; Senta, I.; Ahel, M.; Gros, M.; Petrović, M.; Barcelo, D.; Müller, J.; Knepper, T.; Martí, I.; Ventura, F.; Jovančić, P.; Jabučar, D. Occurrence and Fate of Emerging Wastewater Contaminants in Western Balkan Region. *Sci. Total Environ.* **2008**, *399* (1–3), 66–77. https://doi.org/10.1016/j.scitotenv.2008.03.003.

(80) Shao, B.; Chen, D.; Zhang, J.; Wu, Y.; Sun, C. Determination of 76 Pharmaceutical Drugs by Liquid Chromatography-Tandem Mass Spectrometry in Slaughterhouse Wastewater. *J. Chromatogr. A* **2009**, *1216* (47), 8312–8318. https://doi.org/10.1016/j.chroma.2009.08.038.

(81) Nelson, E. D.; Do, H.; Lewis, R. S.; Carr, S. A. Diurnal Variability of Pharmaceutical, Personal Care Product, Estrogen and Alkylphenol Concentrations in Effluent from a Tertiary Wastewater Treatment Facility. *Environ. Sci. Technol.* **2011**, *45* (4), 1228–1234. https://doi.org/10.1021/es102452f.

(82) Miklos, D. B.; Remy, C.; Jekel, M.; Linden, K. G.; Drewes, J. E.; Hübner, U. Evaluation of Advanced Oxidation Processes for Water and Wastewater Treatment – A Critical Review. *Water Res.* **2018**, *139*, 118–131. https://doi.org/10.1016/j.watres.2018.03.042.

(83) Schmidt, T. C. Recent Trends in Water Analysis Triggering Future Monitoring of Organic Micropollutants. *Anal. Bioanal. Chem.* **2018**, *410* (17), 3933–3941. https://doi.org/10.1007/s00216-018-1015-9.

(84) Zazo, J. A.; Casas, J. A.; Mohedano, A. F.; Gilarranz, M. A.; Rodríguez, J. J. Chemical Pathway and Kinetics of Phenol Oxidation by Fenton's Reagent. *Environ. Sci. Technol.* **2005**, *39* (23), 9295–9302. https://doi.org/10.1021/es050452h.

(85) Rozas, O.; Vidal, C.; Baeza, C.; Jardim, W. F.; Rossner, A.; Mansilla, H. D. Organic Micropollutants (OMPs) in Natural Waters: Oxidation by UV/H2O2 Treatment and Toxicity Assessment. *Water Res.* **2016**, *98*, 109–118. https://doi.org/10.1016/j.watres.2016.03.069.

(86) Richardson, S. D.; Kimura, S. Y. Water Analysis: Emerging Contaminants and Current Issues. *Anal. Chem.* **2016**, *88* (1), 546–582. https://doi.org/10.1021/acs.analchem.5b04493.

(87) Chibwe, L.; Titaley, I. A.; Hoh, E.; Simonich, S. L. M. Integrated Framework for Identifying Toxic Transformation Products in Complex Environmental Mixtures. *Environ. Sci. Technol. Lett.* **2017**, *4* (2), 32–43. https://doi.org/10.1021/acs.estlett.6b00455.

(88) Deborde, M.; von Gunten, U. Reactions of Chlorine with Inorganic and Organic Compounds during Water Treatment-Kinetics and Mechanisms: A Critical Review. *Water Res.* **2008**, *42* (1–2), 13–51. https://doi.org/10.1016/j.watres.2007.07.025.

(89) Chaplin, B. P. Critical Review of Electrochemical Advanced Oxidation Processes for Water Treatment Applications. *Environ. Sci. Process. Impacts* **2014**, *16* (6), 1182–1203. https://doi.org/10.1039/c3em00679d.

(90) Engel, T. *Quantum Chemistry & Spectroscopy*; Pearson Education, Inc, 2013; Vol. 85. https://doi.org/10.1097/00010694-195804000-00011.

(91) Becke, A. D. A New Mixing of Hartree-Fock and Local Density-Functional Theories. *J. Chem. Phys.* **1993**, *98* (2), 1372–1377. https://doi.org/10.1063/1.464304.

(92) Stephens, P. J.; Devlin, F. J.; Chabalowski, C. F.; Frisch, M. J. Ab Initio Calculation of Vibrational Absorption and Circular Dichroism Spectra Using Density Functional Force Fields. *J. Phys. Chem.* **1994**, *98* (45), 11623–11627. https://doi.org/10.1021/j100096a001.

(93) Zhao, Y.; Truhlar, D. G. A New Local Density Functional for Main-Group Thermochemistry, Transition Metal Bonding, Thermochemical Kinetics, and Noncovalent Interactions. *J. Chem. Phys.* **2006**, *125* (19). https://doi.org/10.1063/1.2370993.

(94) Minakata, D.; Crittenden, J. Linear Free Energy Relationships between Aqueous

Phase Hydroxyl Radical Reaction Rate Constants and Free Energy of Activation. *Environ. Sci. Technol.* **2011**, *45* (8), 3479–3486. https://doi.org/10.1021/es1020313.

(95) Guo, X.; Minakata, D.; Niu, J.; Crittenden, J. Computer-Based First-Principles Kinetic Modeling of Degradation Pathways and Byproduct Fates in Aqueous-Phase Advanced Oxidation Processes. *Environ. Sci. Technol.* **2014**, *48* (10), 5718–5725. https://doi.org/10.1021/es500359g.

(96) Zimmermann, S. G.; Wittenwiler, M.; Hollender, J.; Krauss, M.; Ort, C.; Siegrist, H.; von. Kinetic Assessment and Modeling of an Ozonation Step for Full-Scale Municipal Wastewater Treatment : Micropollutant Oxidation , by-Product Formation and Disinfection. *Water Res.* **2010**, *45* (2), 605–617. https://doi.org/10.1016/j.watres.2010.07.080.

(97) Lee, Y.; Kovalova, L.; McArdell, C. S.; von Gunten, U. Prediction of Micropollutant Elimination during Ozonation of a Hospital Wastewater Effluent. *Water Res.* **2014**, *64*, 134–148. https://doi.org/10.1016/j.watres.2014.06.027.

(98) Tentscher, P. R.; Lee, M.; Von Gunten, U. Micropollutant Oxidation Studied by Quantum Chemical Computations: Methodology and Applications to Thermodynamics, Kinetics, and Reaction Mechanisms. *Acc. Chem. Res.* **2019**, *52* (3), 605–614. https://doi.org/10.1021/acs.accounts.8b00610.

(99) Domingo, L. R. Molecular Electron Density Theory: A Modern View of Reactivity in Organic Chemistry. *Molecules* **2016**, *21* (10), 1–15. https://doi.org/10.3390/molecules21101319.

(100) Yang, W.; Mortier, W. J. The Use of Global and Local Molecular Parameters for the Analysis of the Gas-Phase Basicity of Amines. *J. Am. Chem. Soc.* **1986**, *108* (19), 5708–5711. https://doi.org/10.1021/ja00279a008.

(101) Jia, L.; Shen, Z.; Su, P. Relationship between Reaction Rate Constants of Organic Pollutants and Their Molecular Descriptors during Fenton Oxidation and in Situ Formed Ferric-Oxyhydroxides. *J. Environ. Sci. (China)* **2016**, *43*, 257–264. https://doi.org/10.1016/j.jes.2015.10.019.

(102) Zhu, H.; Guo, W.; Shen, Z.; Tang, Q.; Ji, W.; Jia, L. QSAR Models for Degradation of Organic Pollutants in Ozonation Process under Acidic Condition. *Chemosphere* **2015**, *119*, 65–71.

https://doi.org/10.1016/j.chemosphere.2014.05.068.

(103) Liu, W.; Li, Y.; Liu, F.; Jiang, W.; Zhang, D.; Liang, J. Visible-Light-Driven Photocatalytic Degradation of Diclofenac by Carbon Quantum Dots Modified Porous g-C3N4: Mechanisms, Degradation Pathway and DFT Calculation. *Water Res.* **2019**, *150*, 431–441. https://doi.org/10.1016/j.watres.2018.12.001.

(104) Mvula, E.; Schuchmann, M. N.; Von Sonntag, C. Reactions of Phenol-OH-Adduct Radicals. Phenoxyl Radical Formation by Water Elimination vs. Oxidation by Dioxygen. *J. Chem. Soc. Perkin Trans. 2* **2001**, No. 3, 264–268. https://doi.org/10.1039/b008434o.

(105) *Advanced Oxidation Processes for Water Treatment - Fundamentals and Applications*; Stefan, M. I., Ed.; IWA Publishing, 2017; Vol. 16. https://doi.org/10.2166/9781780407197.

(106) Minakata, D.; Kamath, D.; Maetzold, S. Mechanistic Insight into the Reactivity of Chlorine-Derived Radicals in the Aqueous-Phase UV-Chlorine Advanced Oxidation Process: Quantum Mechanical Calculations. *Environ. Sci. Technol.* **2017**, *51* (12), 6918–6926. https://doi.org/10.1021/acs.est.7b00507.

(107) Galano, A.; Alvarez-Idaboy, J. R. Glutathione: Mechanism and Kinetics of Its Non-Enzymatic Defense Action against Free Radicals. *RSC Adv.* **2011**, *1* (9), 1763–1771. https://doi.org/10.1039/c1ra00474c.

(108) Luo, S.; Gao, L.; Wei, Z.; Spinney, R.; Dionysiou, D. D.; Hu, W. P.; Chai, L.; Xiao, R. Kinetic and Mechanistic Aspects of Hydroxyl Radical–mediated Degradation of Naproxen and Reaction Intermediates. *Water Res.* **2018**, *137*, 233–241. https://doi.org/10.1016/j.watres.2018.03.002.

(109) Minakata, D.; Song, W.; Mezyk, S. P.; Cooper, W. J. Experimental and Theoretical Studies on Aqueous-Phase Reactivity of Hydroxyl Radicals with Multiple Carboxylated and Hydroxylated Benzene Compounds. *Phys. Chem. Chem. Phys.* **2015**, *17* (17), 11796–11812. https://doi.org/10.1039/c5cp00861a.

(110) Goto, H.; Nakayama, N.; Ohta, K.; Obata, S. Conflex 8. CONFLEX Corporation: Tokyo, Japan 2017. http://www.conflex.co.jp/product_conflex_new.html.

(111) Frisch, M. J.; Trucks, G. W.; Schlegel, H. B.; Scuseria, G. E.; Robb, M. A.; Cheeseman, J. R.; Scalmani, G.; Barone, V.; Petersson, G. A.; Nakatsuji, H.; Li, X.; Caricato, M.; Marenich, A. V.; Bloino, J.; Janesko, B. G.; Gomperts, R.;

Mennucci, B.; Hratch, D. J. Gaussian 16, Revision B.01. Gaussian, Inc.: Wallingford CT 2016. https://gaussian.com/.

(112) Dennington, R.; Keith, T. A.; Millam, J. M. GaussView 6. Semichem Inc: Shawnee Mission, KS 2016. https://gaussian.com/gaussview6/.

(113) Marenich, A. V.; Cramer, C. J.; Truhlar, D. G. Universal Solvation Model Based on Solute Electron Density and on a Continuum Model of the Solvent Defined by the Bulk Dielectric Constant and Atomic Surface Tensions. *J. Phys. Chem. B* **2009**, *113* (18), 6378–6396. https://doi.org/10.1021/jp810292n.

(114) Ma, Y.; Liang, J.; Zhao, D.; Chen, Y. L.; Shen, J.; Xiong, B. Condensed Fukui Function Predicts Innate C-H Radical Functionalization Sites on Multi-Nitrogen Containing Fused Arenes. *RSC Adv.* **2014**, *4* (33), 17262–17264. https://doi.org/10.1039/c4ra01853b.

(115) Wiberg, K. B.; Rablen, P. R. Atomic Charges. *J. Org. Chem.* **2018**, *83* (24), 15463–15469. https://doi.org/10.1021/acs.joc.8b02740.

(116) Martin, F.; Zipse, H. Charge Distribution in the Water Molecule -A Comparison of Methods. *J. Comput. Chem.* **2005**, *26* (1), 97–105. https://doi.org/10.1002/jcc.20157.

(117) Elhorri, A. M.; Belaid, K. D.; Zouaoui-Rabah, M.; Chadli, R. Theoretical Study of the Azo Dyes Dissociation by Advanced Oxidation Using Fukui Indices. DFT Calculations. *Comput. Theor. Chem.* **2018**, *1130*, 98–106. https://doi.org/10.1016/j.comptc.2018.03.018.

(118) Mendoza-Huizar, L. H.; Rios-Reyes, C. H. Chemical Reactivity of Atrazine Employing the Fukui Function. *J. Mex. Chem. Soc.* **2011**, *55* (3), 142–147.

(119) Vargas-Sánchez, R. D.; Mendoza-Wilson, A. M.; Balandrán-Quintana, R. R.; Torrescano-Urrutia, G. R.; Sánchez-Escalante, A. Study of the Molecular Structure and Chemical Reactivity of Pinocembrin by DFT Calculations. *Comput. Theor. Chem.* **2015**, *1058*, 21–27. https://doi.org/10.1016/j.comptc.2015.01.014.

(120) HPC System Inc. Reaction plus Pro. HPC System Inc. https://www.hpc.co.jp/eng/product_Reactionplus.html.

(121) Henkelman, G.; Jónsson, H. Improved Tangent Estimate in the Nudged Elastic Band Method for Finding Minimum Energy Paths and Saddle Points. *J. Chem.*

Phys. **2000**, *113* (22), 9978–9985. https://doi.org/10.1063/1.1323224.

(122) Mujika, J. I.; Uranga, J.; Matxain, J. M. Computational Study on the Attack of ·OH Radicals on Aromatic Amino Acids. *Chem. - A Eur. J.* **2013**, *19* (21), 6862–6873. https://doi.org/10.1002/chem.201203862.

(123) Wu, C.; De Visscher, A.; Gates, I. D. Reactions of Hydroxyl Radicals with Benzoic Acid and Benzoate. *RSC Adv.* **2017**, *7* (57), 35776–35785. https://doi.org/10.1039/c7ra05488b.

(124) Rappoport, Z. *The Chemistry of Phenols*; John Wiley & Sons, Ltd, 2003; Vol. 116. https://doi.org/10.1038/116799a0.

(125) Bushnell, E. A. C.; Gauld, J. W. An Assessment of Pure, Hybrid, Meta, and Hybrid-Meta GGA Density Functional Theory Methods for Open-Shell Systems: The Case of the Nonheme Iron Enzyme 8R-LOX. *J. Comput. Chem.* **2013**, *34* (2), 141–148. https://doi.org/10.1002/jcc.23114.

(126) von Sonntag, C.; Schuchmann, H. -P. The Elucidation of Peroxyl Radical Reactions in Aqueous Solution with the Help of Radiation-Chemical Methods. *Angew. Chemie Int. Ed. English* **1991**, *30* (10), 1229–1253. https://doi.org/10.1002/anie.199112291.

(127) Zhou, P.; Ayers, P. W.; Liu, S.; Li, T. Natural Orbital Fukui Function and Application in Understanding Cycloaddition Reaction Mechanisms. *Phys. Chem. Chem. Phys.* **2012**, *14* (28), 9890–9896. https://doi.org/10.1039/c2cp40488e.

(128) Kroflič, A.; Schaefer, T.; Huš, M.; Phuoc Le, H.; Otto, T.; Herrmann, H. OH Radicals Reactivity towards Phenol-Related Pollutants in Water: Temperature Dependence of the Rate Constants and Novel Insights into the [OH-Phenol] Adduct Formation. *Phys. Chem. Chem. Phys.* **2020**, *22* (3), 1324–1332. https://doi.org/10.1039/c9cp05533a.

(129) Winterbourn, C. C.; Kettle, A. J. Radical-Radical Reactions of Superoxide: A Potential Route to Toxicity. *Biochem. Biophys. Res. Commun.* **2003**, *305* (3), 729–736. https://doi.org/10.1016/S0006-291X(03)00810-6.

(130) Galano, A.; Alvarez-Idaboy, J. R. A Computational Methodology for Accurate Predictions of Rate Constants in Solution: Application to the Assessment of Primary Antioxidant Activity. *J. Comput. Chem.* **2013**, *34* (28), 2430–2445. https://doi.org/10.1002/jcc.23409.

(131) Trogolo, D.; Mishra, B. K.; Heeb, M. B.; Von Gunten, U.; Arey, J. S. Molecular Mechanism of NDMA Formation from N, N-Dimethylsulfamide during Ozonation: Quantum Chemical Insights into a Bromide-Catalyzed Pathway. *Environ. Sci. Technol.* **2015**, *49* (7), 4163–4175. https://doi.org/10.1021/es504407h.

(132) Zhao, Y.; Tishchenko, O.; Gour, J. R.; Li, W.; Lutz, J. J.; Piecuch, P.; Truhlar, D. G. Thermochemical Kinetics for Multireference Systems: Addition Reactions of Ozone. *J. Phys. Chem. A* **2009**, *113* (19), 5786–5799. https://doi.org/10.1021/jp811054n.

(133) Kristyán, S.; Pulay, P. Can (Semi)Local Density Functional Theory Account for the London Dispersion Forces? *Chem. Phys. Lett.* **1994**, *229* (3), 175–180. https://doi.org/10.1016/0009-2614(94)01027-7.

(134) Tishchenko, O.; Truhlar, D. G. Benchmark Ab Initio Calculations of the Barrier Height and Transition-State Geometry for Hydrogen Abstraction from a Phenolic Antioxidant by a Peroxy Radical and Its Use to Assess the Performance of Density Functionals. *J. Phys. Chem. Lett.* **2012**, *3* (19), 2834–2839. https://doi.org/10.1021/jz3011817.

(135) Kirklin, S.; Saal, J. E.; Meredig, B.; Thompson, A.; Doak, J. W.; Aykol, M.; Rühl, S.; Wolverton, C. The Open Quantum Materials Database (OQMD): Assessing the Accuracy of DFT Formation Energies. *npj Comput. Mater.* **2015**, *1* (November). https://doi.org/10.1038/npjcompumats.2015.10.

(136) Buxton, G. V.; Greenstock, C. L.; Helman, W. P.; Ross, A. B. Critical Review of Rate Constants for Reactions of Hydrated Electrons, Hydrogen Atoms and Hydroxyl Radicals (·OH/·O− in Aqueous Solution. *J. Phys. Chem. Ref. Data* **1988**, *17* (2), 513–886. https://doi.org/10.1063/1.555805.

(137) Milosavljevic, B. H.; La Verne, J. A.; Pimblott, S. M. Rate Coefficient Measurements of Hydrated Electrons and Hydroxyl Radicals with Chlorinated Ethanes in Aqueous Solutions. *J. Phys. Chem. A* **2005**, *109* (34), 7751–7756. https://doi.org/10.1021/jp051249b.

(138) Mardirossian, N.; Head-Gordon, M. How Accurate Are the Minnesota Density Functionals for Noncovalent Interactions, Isomerization Energies, Thermochemistry, and Barrier Heights Involving Molecules Composed of Main-

Group Elements? *J. Chem. Theory Comput.* **2016**, *12* (9), 4303–4325. https://doi.org/10.1021/acs.jctc.6b00637.

(139) Astuti, M. P.; Rangsivek, R.; Padhye, L. P. Laboratory and Pilot-Scale UV, UV/H2O2, and Granular Activated Carbon (GAC) Treatments for Simultaneous Removal of Five Chemicals of Emerging Concerns (CECs) in Water. *J. Water Process Eng.* **2022**, *47* (February), 102730. https://doi.org/10.1016/j.jwpe.2022.102730.

(140) Cibati, A.; Gonzalez-Olmos, R.; Rodriguez-Mozaz, S.; Buttiglieri, G. Unravelling the Performance of UV/H2O2 on the Removal of Pharmaceuticals in Real Industrial, Hospital, Grey and Urban Wastewaters. *Chemosphere* **2022**, *290* (October 2021), 133315. https://doi.org/10.1016/j.chemosphere.2021.133315.

(141) Li, K.; Hokanson, D. R.; Crittenden, J. C.; Trussell, R. R.; Minakata, D. Evaluating UV/H2O2 Processes for Methyl Tert-Butyl Ether and Tertiary Butyl Alcohol Removal: Effect of Pretreatment Options and Light Sources. *Water Res.* **2008**, *42* (20), 5045–5053. https://doi.org/10.1016/j.watres.2008.09.017.

(142) Keen, O. S.; McKay, G.; Mezyk, S. P.; Linden, K. G.; Rosario-Ortiz, F. L. Identifying the Factors That Influence the Reactivity of Effluent Organic Matter with Hydroxyl Radicals. *Water Res.* **2014**, *50*, 408–419. https://doi.org/10.1016/j.watres.2013.10.049.

(143) Yang, X.; Rosario-Ortiz, F. L.; Lei, Y.; Pan, Y.; Lei, X.; Westerhoff, P. Multiple Roles of Dissolved Organic Matter in Advanced Oxidation Processes. *Environ. Sci. Technol.* **2022**, *56* (16), 11111–11131. https://doi.org/10.1021/acs.est.2c01017.

(144) Brame, J.; Long, M.; Li, Q.; Alvarez, P. Inhibitory Effect of Natural Organic Matter or Other Background Constituents on Photocatalytic Advanced Oxidation Processes: Mechanistic Model Development and Validation. *Water Res.* **2015**, *84*, 362–371. https://doi.org/10.1016/j.watres.2015.07.044.

(145) Chen, D. Z.; Jin, X. J.; Chen, J.; Ye, J. X.; Jiang, N. X.; Chen, J. M. Intermediates and Substrate Interaction of 1,4-Dioxane Degradation by the Effective Metabolizer Xanthobacter Flavus DT8. *Int. Biodeterior. Biodegrad.* **2016**, *106*, 133–140. https://doi.org/10.1016/j.ibiod.2015.09.018.

(146) Spencer, R. G. M.; Bolton, L.; Baker, A. Freeze/Thaw and PH Effects on

Freshwater Dissolved Organic Matter Fluorescence and Absorbance Properties from a Number of UK Locations. *Water Res.* **2007**, *41* (13), 2941–2950. https://doi.org/10.1016/j.watres.2007.04.012.

(147) Hudson, N.; Baker, A.; Ward, D.; Reynolds, D. M.; Brunsdon, C.; Carliell-Marquet, C.; Browning, S. Can Fluorescence Spectrometry Be Used as a Surrogate for the Biochemical Oxygen Demand (BOD) Test in Water Quality Assessment? An Example from South West England. *Sci. Total Environ.* **2008**, *391* (1), 149–158. https://doi.org/10.1016/j.scitotenv.2007.10.054.

(148) Bieroza, M.; Baker, A.; Bridgeman, J. Relating Freshwater Organic Matter Fluorescence to Organic Carbon Removal Efficiency in Drinking Water Treatment. *Sci. Total Environ.* **2009**, *407* (5), 1765–1774. https://doi.org/10.1016/j.scitotenv.2008.11.013.

(149) Peiris, R. H.; Hallé, C.; Budman, H.; Moresoli, C.; Peldszus, S.; Huck, P. M.; Legge, R. L. Identifying Fouling Events in a Membrane-Based Drinking Water Treatment Process Using Principal Component Analysis of Fluorescence Excitation-Emission Matrices. *Water Res.* **2010**, *44* (1), 185–194. https://doi.org/10.1016/j.watres.2009.09.036.

(150) Corin, N.; Backhand, P.; Kulovaara, M. Degradation Products Formed during UV-Irradiation of Humic Waters. *Chemosphere* **1996**, *33* (2), 245–255. https://doi.org/10.1016/0045-6535(96)00167-1.

(151) Buchanan, W.; Roddick, F.; Porter, N.; Drikas, M. Fractionation of UV and VUV Pretreated Natural Organic Matter from Drinking Water. *Environ. Sci. Technol.* **2005**, *39* (12), 4647–4654. https://doi.org/10.1021/es048489+.

(152) Lee, M.; Zimmermann-Steffens, S. G.; Arey, J. S.; Fenner, K.; Von Gunten, U. Development of Prediction Models for the Reactivity of Organic Compounds with Ozone in Aqueous Solution by Quantum Chemical Calculations: The Role of Delocalized and Localized Molecular Orbitals. *Environ. Sci. Technol.* **2015**, *49* (16), 9925–9935. https://doi.org/10.1021/acs.est.5b00902.

(153) Davaritouchaee, M.; Hiscox, W. C.; Terrell, E.; Mancini, R. J.; Chen, S. Mechanistic Studies of Milled and Kraft Lignin Oxidation by Radical Species. *Green Chem.* **2020**, *22* (4), 1182–1197. https://doi.org/10.1039/c9gc04162a.

(154) Miranda, M. L.; Osterholz, H.; Giebel, H. A.; Bruhnke, P.; Dittmar, T.; Zielinski,

O. Impact of UV Radiation on DOM Transformation on Molecular Level Using FT-ICR-MS and PARAFAC. *Spectrochim. Acta - Part A Mol. Biomol. Spectrosc.* **2020**, *230*, 118027. https://doi.org/10.1016/j.saa.2020.118027.

(155) Mehmood, C. T.; Lu, C.; Maqbool, T.; Xiao, Y.; Zhong, Z. Molecular Transformations of Dissolved Organic Matter during UV/O3-Assisted Membrane Filtration of UASB-Treated Real Textile Wastewater. *Chemosphere* **2022**, *307* (P4), 136101. https://doi.org/10.1016/j.chemosphere.2022.136101.

(156) Varanasi, L.; Coscarelli, E.; Khaksari, M.; Mazzoleni, L. R.; Minakata, D. Transformations of Dissolved Organic Matter Induced by UV Photolysis, Hydroxyl Radicals, Chlorine Radicals, and Sulfate Radicals in Aqueous-Phase UV-Based Advanced Oxidation Processes. *Water Res.* **2018**, *135*, 22–30. https://doi.org/10.1016/j.watres.2018.02.015.

(157) Zhang, B.; Shan, C.; Wang, S.; Fang, Z.; Pan, B. Unveiling the Transformation of Dissolved Organic Matter during Ozonation of Municipal Secondary Effluent Based on FT-ICR-MS and Spectral Analysis. *Water Res.* **2021**, *188*, 116484. https://doi.org/10.1016/j.watres.2020.116484.

(158) Xiang, Y.; Gonsior, M.; Schmitt-Kopplin, P.; Shang, C. Influence of the UV/H2O2Advanced Oxidation Process on Dissolved Organic Matter and the Connection between Elemental Composition and Disinfection Byproduct Formation. *Environ. Sci. Technol.* **2020**, *54* (23), 14964–14973. https://doi.org/10.1021/acs.est.0c03220.

(159) Zhang, S.; Hao, Z.; Liu, J.; Croué, J. P. Molecular-Level Investigation into UV-Induced Transformation of Hydrophobic Aquatic Dissolved Organic Matter. *Sci. Total Environ.* **2022**, *842* (April). https://doi.org/10.1016/j.scitotenv.2022.156959.

(160) Zhang, S.; Hao, Z.; Liu, J.; Gutierrez, L.; Croué, J. P. Molecular Insights into the Reactivity of Aquatic Natural Organic Matter towards Hydroxyl (•OH) and Sulfate (SO4•−) Radicals Using FT-ICR MS. *Chem. Eng. J.* **2021**, *425* (June). https://doi.org/10.1016/j.cej.2021.130622.

(161) Remucal, C. K.; Salhi, E.; Walpen, N.; Von Gunten, U. Molecular-Level Transformation of Dissolved Organic Matter during Oxidation by Ozone and Hydroxyl Radical. *Environ. Sci. Technol.* **2020**, *54* (16), 10351–10360.

https://doi.org/10.1021/acs.est.0c03052.

(162) Song, Z. M.; Yang, L. L.; Lu, Y.; Wang, C.; Liang, J. K.; Du, Y.; Li, X. Z.; Hu, Q.; Guan, Y. T.; Wu, Q. Y. Characterization of the Transformation of Natural Organic Matter and Disinfection Byproducts after Chlorination, Ultraviolet Irradiation and Ultraviolet Irradiation/Chlorination Treatment. *Chem. Eng. J.* **2021**, *426* (June). https://doi.org/10.1016/j.cej.2021.131916.

(163) Ruan, X.; Xiang, Y.; Shang, C.; Cheng, S.; Liu, J.; Hao, Z.; Yang, X. Molecular Characterization of Transformation and Halogenation of Natural Organic Matter during the UV/Chlorine AOP Using FT-ICR Mass Spectrometry. *J. Environ. Sci. (China)* **2021**, *102*, 24–36. https://doi.org/10.1016/j.jes.2020.08.028.

(164) Jennings, E. K.; Sierra Olea, M.; Kaesler, J. M.; Hübner, U.; Reemtsma, T.; Lechtenfeld, O. J. Stable Isotope Labeling for Detection of Ozonation Byproducts in Effluent Organic Matter with FT-ICR-MS. *Water Res.* **2023**, *229* (November 2022), 119477. https://doi.org/10.1016/j.watres.2022.119477.

(165) Wang, H.; Ge, D.; Cheng, Z.; Zhu, N.; Yuan, H.; Lou, Z. Improved Understanding of Dissolved Organic Matter Transformation in Concentrated Leachate Induced by Hydroxyl Radicals and Reactive Chlorine Species. *J. Hazard. Mater.* **2020**, *387* (October 2019), 121702. https://doi.org/10.1016/j.jhazmat.2019.121702.

(166) Spahr, S.; Von Gunten, U.; Hofstetter, T. B. Carbon, Hydrogen, and Nitrogen Isotope Fractionation Trends in N-Nitrosodimethylamine Reflect the Formation Pathway during Chloramination of Tertiary Amines. *Environ. Sci. Technol.* **2017**, *51* (22), 13170–13179. https://doi.org/10.1021/acs.est.7b03919.

(167) Brunner, A. M.; Vughs, D.; Siegers, W.; Bertelkamp, C.; Hofman-Caris, R.; Kolkman, A.; ter Laak, T. Monitoring Transformation Product Formation in the Drinking Water Treatments Rapid Sand Filtration and Ozonation. *Chemosphere* **2019**, *214*, 801–811. https://doi.org/10.1016/j.chemosphere.2018.09.140.

(168) Fu, Q. L.; Fujii, M.; Watanabe, A.; Kwon, E. Formula Assignment Algorithm for Deuterium-Labeled Ultrahigh-Resolution Mass Spectrometry: Implications of the Formation Mechanism of Halogenated Disinfection Byproducts. *Anal. Chem.* **2022**, *94* (3), 1717–1725. https://doi.org/10.1021/acs.analchem.1c04298.

(169) Clarke, S. Ultraviolet Light Disinfection in the Use of Individual Water

Purification Devices. *U.S Army Public Heal. Command* **2006**, 1–12.

(170) Marshall, A. G.; Hendrickson, C. L.; Jackson, G. S. Fourier Transform Ion Cyclotron Resonance Mass Spectrometry: A Primer. *Mass Spectrom. Rev.* **1998**, *17* (1), 1–35. https://doi.org/10.1002/(SICI)1098-2787(1998)17:1<1::AID-MAS1>3.0.CO;2-K.

(171) Liu, J.; Wang, C.; Hao, Z.; Kondo, G.; Fujii, M.; Fu, Q. L.; Wei, Y. Comprehensive Understanding of DOM Reactivity in Anaerobic Fermentation of Persulfate-Pretreated Sewage Sludge via FT-ICR Mass Spectrometry and Reactomics Analysis. *Water Res.* **2023**, *229* (October 2022), 119488. https://doi.org/10.1016/j.watres.2022.119488.

(172) Chen, T.; Guestrin, C. XGBoost: A Scalable Tree Boosting System. *Proc. ACM SIGKDD Int. Conf. Knowl. Discov. Data Min.* **2016**, *13-17-Augu*, 785–794. https://doi.org/10.1145/2939672.2939785.

(173) Liu, Y.; Just, A. SHAPforxgboost: SHAP Plots for "XGBoost." 2020. https://github.com/liuyanguu/SHAPforxgboost/.

(174) Bastian, M.; Heymann, S.; Jacomy, M. Gephi: An Open Source Software for Exploring and Manipulating Networks. International AAAI Conference on Weblogs and Social Media 2009.

(175) Zhang, B.; Wang, X.; Fang, Z.; Wang, S.; Shan, C.; Wei, S.; Pan, B. Unravelling Molecular Transformation of Dissolved Effluent Organic Matter in UV/H2O2, UV/Persulfate, and UV/Chlorine Processes Based on FT-ICR-MS Analysis. *Water Res.* **2021**, *199*, 117158. https://doi.org/10.1016/j.watres.2021.117158.

(176) Wu, Q. Y.; Zhou, T. H.; Du, Y.; Ye, B.; Wang, W. L.; Hu, H. Y. Characterizing the Molecular Weight Distribution of Dissolved Organic Matter by Measuring the Contents of Electron-Donating Moieties, UV Absorbance, and Fluorescence Intensity. *Environ. Int.* **2020**, *137* (February). https://doi.org/10.1016/j.envint.2020.105570.

(177) John, R. H.; Stubbins, A.; Ritchie, J. D.; Minor, E. C.; Kieber, D. J.; Mopper, K. Erratum: Absorption Spectral Slopes and Slope Ratios as Indicators of Molecular Weight, Source, and Photobleaching of Chromophoric Dissolved Organic Matter (Limnology and Oceanography 53 955-969). *Limnol. Oceanogr.* **2009**, *54* (3), 1023. https://doi.org/10.4319/lo.2009.54.3.1023.

(178) Mostovaya, A.; Hawkes, J. A.; Dittmar, T.; Tranvik, L. J. Molecular Determinants of Dissolved Organic Matter Reactivity in Lake Water. *Front. Earth Sci.* **2017**, *5* (December), 1–13. https://doi.org/10.3389/feart.2017.00106.

(179) Fu, Q. L.; Fujii, M.; Kwon, E. Development and Application of a High-Precision Algorithm for Nontarget Identification of Organohalogens Based on Ultrahigh-Resolution Mass Spectrometry. *Anal. Chem.* **2020**, *92* (20), 13989–13996. https://doi.org/10.1021/acs.analchem.0c02899.

(180) Rayaroth, M. P.; Aravindakumar, C. T.; Shah, N. S.; Boczkaj, G. Advanced Oxidation Processes (AOPs) Based Wastewater Treatment - Unexpected Nitration Side Reactions - a Serious Environmental Issue: A Review. *Chem. Eng. J.* **2022**, *430* (P4), 133002. https://doi.org/10.1016/j.cej.2021.133002.

(181) Flyunt, R.; Makogon, O.; Schuchmann, M. N.; Asmus, K. D.; Von Sonntag, C. OH-Radical-Induced Oxidation of Methanesulfinic Acid. The Reactions of the Methanesulfonyl Radical in the Absence and Presence of Dioxygen. *J. Chem. Soc. Perkin Trans. 2* **2001**, No. 5, 787–792. https://doi.org/10.1039/b009631h.

(182) Vluymans, S. Learning from Imbalanced Data. *Stud. Comput. Intell.* **2019**, *807* (9), 81–110. https://doi.org/10.1007/978-3-030-04663-7_4.

(183) Waggoner, D. C.; Hatcher, P. G. Hydroxyl Radical Alteration of HPLC Fractionated Lignin: Formation of New Compounds from Terrestrial Organic Matter. *Org. Geochem.* **2017**, *113*, 315–325. https://doi.org/10.1016/j.orggeochem.2017.07.011.

(184) Geng, W.; Wei, Y.; Ke, Y.; Qin, J.; Yu, X.; Guo, X.; Long, M. Unveiling Molecular Transformations of Soil Organic Matter after Remediation by Chemical Oxidation Based on ESI-FT-ICR-MS Analysis. *ACS ES T Eng.* **2022**. https://doi.org/10.1021/acsestengg.2c00423.

(185) Koopmann, A.-K.; Schuster, C.; Torres-Rodríguez, J.; Kain, S.; Pertl-Obermayer, H.; Petutschnigg, A.; Hüsing, N. Tannin-Based Hybrid Materials and Their. *Molecules* **2020**, *25* (21), 4910.

(186) Wu, T. S.; Syu, L. Y.; Lin, C. N.; Lin, B. H.; Liao, Y. H.; Weng, S. C.; Huang, Y. J.; Jeng, H. T.; Lu, S. Y.; Chang, S. L.; Soo, Y. L. Enhancement of Catalytic Activity by UV-Light Irradiation in CeO2 Nanocrystals. *Sci. Rep.* **2019**, *9* (1), 2–8. https://doi.org/10.1038/s41598-019-44543-2.

(187) Arbenz, A.; Avérous, L. Chemical Modification of Tannins to Elaborate Aromatic Biobased Macromolecular Architectures. *Green Chem.* **2015**, *17* (5), 2626–2646. https://doi.org/10.1039/c5gc00282f.

(188) Jezuita, A.; Ejsmont, K.; Szatylowicz, H. Substituent Effects of Nitro Group in Cyclic Compounds. *Struct. Chem.* **2021**, *32* (1), 179–203. https://doi.org/10.1007/s11224-020-01612-x.

(189) Mitroka, S.; Zimmeck, S.; Troya, D.; Tanko, J. M. How Solvent Modulates Hydroxyl Radical Reactivity in Hydrogen Atom Abstractions. *J. Am. Chem. Soc.* **2010**, *132* (9), 2907–2913. https://doi.org/10.1021/ja903856t.

(190) LaRowe, D. E.; Van Cappellen, P. Degradation of Natural Organic Matter: A Thermodynamic Analysis. *Geochim. Cosmochim. Acta* **2011**, *75* (8), 2030–2042. https://doi.org/10.1016/j.gca.2011.01.020.

(191) Solà, M. Aromaticity Rules. *Nat. Chem.* **2022**, *14* (6), 585–590. https://doi.org/10.1038/s41557-022-00961-w.

(192) Waggoner, D. C.; Chen, H.; Willoughby, A. S.; Hatcher, P. G. Formation of Black Carbon-like and Alicyclic Aliphatic Compounds by Hydroxyl Radical Initiated Degradation of Lignin. *Org. Geochem.* **2015**, *82*, 69–76. https://doi.org/10.1016/j.orggeochem.2015.02.007.

(193) Nauser, T.; Gebicki, J. M. Addition of Carbon-Centered Radicals to Aromatic Antioxidants: Mechanistic Aspects. *Phys. Chem. Chem. Phys.* **2020**, *22* (42), 24572–24582. https://doi.org/10.1039/d0cp04469e.

(194) Meng, X.; Crestini, C.; Ben, H.; Hao, N.; Pu, Y.; Ragauskas, A. J.; Argyropoulos, D. S. Determination of Hydroxyl Groups in Biorefinery Resources via Quantitative 31P NMR Spectroscopy. *Nat. Protoc.* **2019**, *14* (9), 2627–2647. https://doi.org/10.1038/s41596-019-0191-1.

(195) Li, J.; Zhang, X.; Fan, W. Y.; Yao, M. C.; Sheng, G. P. Dissolved Organic Matter Dominating the Photodegradation of Free DNA Bases in Aquatic Environments. *Water Res.* **2020**, *179*, 115885. https://doi.org/10.1016/j.watres.2020.115885.

(196) Dizhbite, T.; Telysheva, G.; Jurkjane, V.; Viesturs, U. Characterization of the Radical Scavenging Activity of Lignins - Natural Antioxidants. *Bioresour. Technol.* **2004**, *95* (3), 309–317. https://doi.org/10.1016/j.biortech.2004.02.024.

(197) Qi, Y.; Fu, P.; Li, S.; Ma, C.; Liu, C.; Volmer, D. A. Assessment of Molecular

Diversity of Lignin Products by Various Ionization Techniques and High-Resolution Mass Spectrometry. *Sci. Total Environ.* **2020**, *713*, 136573. https://doi.org/10.1016/j.scitotenv.2020.136573.

(198) Bonawitz, N. D.; Chapple, C. The Genetics of Lignin Biosynthesis: Connecting Genotype to Phenotype. *Annu. Rev. Genet.* **2010**, *44* (1), 337–363. https://doi.org/10.1146/annurev-genet-102209-163508.

(199) Freudenberg, K.; Neish, A. C. *Constitution and Biosynthesis of Lignin*, 1st ed.; Springer Berlin, Heidelberg, 1968.

(200) Ludwig, C. H.; Sarkanen, K. *Lignins: Occurrence, Formation, Structure and Reactions*; 1971.

(201) Adler, E. Lignin Chemistry—Past, Present and Future. *Wood Sci. Technol.* **1977**, *11* (3), 169–218. https://doi.org/10.1007/BF00365615.

(202) Whetten, R.; Sederoff, R. Lignin Biosynthesis. *Plant Cell* **1995**, *7* (7), 1001–1013.

(203) Qi, Y.; Hempelmann, R.; Volmer, D. A. Shedding Light on the Structures of Lignin Compounds: Photo-Oxidation under Artificial UV Light and Characterization by High Resolution Mass Spectrometry. *Anal. Bioanal. Chem.* **2016**, *408* (28), 8203–8210. https://doi.org/10.1007/s00216-016-9928-7.

(204) Banoub, J.; Delmas, G. H.; Joly, N.; Mackenzie, G.; Cachet, N.; Benjelloun-Mlayah, B.; Delmas, M. A Critique on the Structural Analysis of Lignins and Application of Novel Tandem Mass Spectrometric Strategies to Determine Lignin Sequencing. *J. Mass Spectrom.* **2015**, *50* (1), 5–48. https://doi.org/10.1002/jms.3541.

(205) Dolk, M.; Pla, F.; Yan, J. F.; McCarthy, J. L. Lignin. 22. Macromolecular Characteristics of Alkali Lignin from Western Hemlock Wood. In *Macromolecules*; 1986; p 1464.

(206) Hedges, J. I.; Keil, R. G.; Benner, R. What Happens to Terrestrial Organic Matter in the Ocean? *Org. Geochem.* **1997**, *27* (5–6), 195–212. https://doi.org/10.1016/S0146-6380(97)00066-1.

(207) Health Canada. Guidance on Natural Organic Matter in Drinking Water. *Gov. Canada* **2019**, 73.

(208) Bugg, T. D. H.; Ahmad, M.; Hardiman, E. M.; Rahmanpour, R. Pathways for

Degradation of Lignin in Bacteria and Fungi. *Nat. Prod. Rep.* **2011**, *28* (12), 1883–1896. https://doi.org/10.1039/c1np00042j.

(209) Thevenot, M.; Dignac, M. F.; Rumpel, C. Fate of Lignins in Soils: A Review. *Soil Biol. Biochem.* **2010**, *42* (8), 1200–1211. https://doi.org/10.1016/j.soilbio.2010.03.017.

(210) Orem, W. H.; Colman, S. M.; Lerch, H. E. Lignin Phenols in Sediments of Lake Baikal, Siberia: Application to Paleoenvironmental Studies. *Org. Geochem.* **1997**, *27* (3–4), 153–172. https://doi.org/10.1016/S0146-6380(97)00079-X.

(211) Li, X.; Zhang, T.; Sun, S.; Lan, H.; Yu, T. Lignin in Marine Environment and Its Analysis-A Review. *J. Ocean Univ. China* **2012**, *11* (4), 501–506. https://doi.org/10.1007/s11802-012-1834-9.

(212) Tareq, S. M.; Kitagawa, H.; Ohta, K. Lignin Biomarker and Isotopic Records of Paleovegetation and Climate Changes from Lake Erhai, Southwest China, since 18.5kaBP. *Quat. Int.* **2011**, *229* (1–2), 47–56. https://doi.org/10.1016/j.quaint.2010.04.014.

(213) Rezende, C. E.; Pfeiffer, W. C.; Martinelli, L. A.; Tsamakis, E.; Hedges, J. I.; Keil, R. G. Lignin Phenols Used to Infer Organic Matter Sources to Sepetiba Bay - RJ, Brasil. *Estuar. Coast. Shelf Sci.* **2010**, *87* (3), 479–486. https://doi.org/10.1016/j.ecss.2010.02.008.

(214) Pempkowiak, J. Limitation of Lignin Derivatives as Biomarkers of Land Derived Organic Matter in the Coastal Marine Sediments. *Oceanologia* **2020**, *62* (3), 374–386. https://doi.org/10.1016/j.oceano.2020.04.004.

(215) Mayer, L. M.; Schick, L. L.; Bianchi, T. S.; Wysocki, L. A. Photochemical Changes in Chemical Markers of Sedimentary Organic Matter Source and Age. *Mar. Chem.* **2009**, *113* (1–2), 123–128. https://doi.org/10.1016/j.marchem.2009.01.006.

(216) Standley, L. J.; Kaplan, L. A. Isolation and Analysis of Lignin-Derived Phenols in Aquatic Humic Substances: Improvements on the Procedures. *Org. Geochem.* **1998**, *28* (11), 689–697. https://doi.org/10.1016/S0146-6380(98)00041-2.

(217) Opsahl, S.; Benner, R. Photochemical Reactivity of Dissolved Lignin in River and Ocean Waters. *Limnol. Oceanogr.* **1998**, *43* (6), 1297–1304. https://doi.org/10.4319/lo.1998.43.6.1297.

(218) Feng, X.; Hills, K. M.; Simpson, A. J.; Whalen, J. K.; Simpson, M. J. The Role of Biodegradation and Photo-Oxidation in the Transformation of Terrigenous Organic Matter. *Org. Geochem.* **2011**, *42* (3), 262–274. https://doi.org/10.1016/j.orggeochem.2011.01.002.

(219) Ma, Y. S.; Chang, C. N.; Chiang, Y. P.; Sung, H. F.; Chao, A. C. Photocatalytic Degradation of Lignin Using Pt/TiO2 as the Catalyst. *Chemosphere* **2008**, *71* (5), 998–1004. https://doi.org/10.1016/j.chemosphere.2007.10.061.

(220) Yurdakal, S.; Palmisano, G.; Loddo, V.; Augugliaro, V.; Palmisano, L. Nanostructured Rutile TiO2 for Selective Photocatalytic Oxidation of Aromatic Alcohols to Aldehydes in Water. *J. Am. Chem. Soc.* **2008**, *130* (5), 1568–1569. https://doi.org/10.1021/ja709989e.

(221) Kaiser, K.; Benner, R. Characterization of Lignin by Gas Chromatography and Mass Spectrometry Using a Simplified CuO Oxidation Method. *Anal. Chem.* **2012**, *84* (1), 459–464. https://doi.org/10.1021/ac202004r.

(222) Mante, O. D.; Rodriguez, J. A.; Babu, S. P. Selective Defunctionalization by TiO2 of Monomeric Phenolics from Lignin Pyrolysis into Simple Phenols. *Bioresour. Technol.* **2013**, *148*, 508–516. https://doi.org/10.1016/j.biortech.2013.09.003.

(223) Sangha, A. K.; Parks, J. M.; Standaert, R. F.; Ziebell, A.; Davis, M.; Smith, J. C. Radical Coupling Reactions in Lignin Synthesis: A Density Functional Theory Study. *J. Phys. Chem. B* **2012**, *116* (16), 4760–4768. https://doi.org/10.1021/jp2122449.

(224) Li, W.; Liu, N.; Li, J.; Wang, B.; Shi, X.; Liang, X.; Yang, M.; Xu, S.; Liu, C. Q. Chemodiversity of Dissolved Organic Matter Is Governed by Microbial Biogeography in Inland Waters. *Environ. Sci. Technol.* **2023**, *57* (20), 7753–7763. https://doi.org/10.1021/acs.est.3c00896.

(225) Hu, A.; Choi, M.; Tanentzap, A. J.; Liu, J.; Jang, K. S.; Lennon, J. T.; Liu, Y.; Soininen, J.; Lu, X.; Zhang, Y.; Shen, J.; Wang, J. Ecological Networks of Dissolved Organic Matter and Microorganisms under Global Change. *Nat. Commun.* **2022**, *13* (1), 1–15. https://doi.org/10.1038/s41467-022-31251-1.

(226) Stadler, M.; Barnard, M. A.; Bice, K.; de Melo, M. L.; Dwivedi, D.; Freeman, E. C.; Garayburu-Caruso, V. A.; Linkhorst, A.; Mateus-Barros, E.; Shi, C.;

Tanentzap, A. J.; Meile, C. Applying the Core-Satellite Species Concept: Characteristics of Rare and Common Riverine Dissolved Organic Matter. *Front. Water* **2023**, *5*. https://doi.org/10.3389/frwa.2023.1156042.

(227) Danczak, R. E.; Chu, R. K.; Fansler, S. J.; Goldman, A. E.; Graham, E. B.; Tfaily, M. M.; Toyoda, J.; Stegen, J. C. Using Metacommunity Ecology to Understand Environmental Metabolomes. *Nat. Commun.* **2020**, *11* (1), 1–16. https://doi.org/10.1038/s41467-020-19989-y.

(228) Boehmke, B.; Greenwell, B. *Hands-On Machine Learning with R*; Taylor and Francis Group, 2020.

(229) Kruve, A.; Kaupmees, K.; Liigand, J.; Leito, I. Negative Electrospray Ionization via Deprotonation: Predicting the Ionization Efficiency. *Anal. Chem.* **2014**, *86* (10), 4822–4830. https://doi.org/10.1021/ac404066v.

(230) Bastian, M.; Heymann, S.; Jacomy, M. Gephi: An Open Source Software for Exploring and Manipulating Networks. BT - International AAAI Conference on Weblogs and Social. *Int. AAAI Conf. Weblogs Soc. Media* **2009**, 361–362.

(231) Lehtola, M. J.; Miettinen, I. T.; Vartiainen, T.; Rantakokko, P.; Hirvonen, A.; Martikainen, P. J. Impact of UV Disinfection on Microbially Available Phosphorus, Organic Carbon, and Microbial Growth in Drinking Water. *Water Res.* **2003**, *37* (5), 1064–1070. https://doi.org/10.1016/S0043-1354(02)00462-1.

(232) Zhao, Q.; Shang, C.; Zhang, X.; Ding, G.; Yang, X. Formation of Halogenated Organic Byproducts during Medium-Pressure UV and Chlorine Coexposure of Model Compounds, NOM and Bromide. *Water Res.* **2011**, *45* (19), 6545–6554. https://doi.org/10.1016/j.watres.2011.09.053.

(233) Ma, R.; Guo, M.; Zhang, X. Recent Advances in Oxidative Valorization of Lignin. *Catal. Today* **2018**, *302* (March 2017), 50–60. https://doi.org/10.1016/j.cattod.2017.05.101.

(234) Dwinandha, D.; Elsamadony, M.; Gao, R.; Fu, Q.-L.; Liu, J.; Fujii, M. *Interpretable Machine Learning and Reactomics Assisted Isotopically Labelled FT-ICR-MS for Exploring Reactivity and Transformation of Natural Organic Matter During UV Photolysis*; 2023.

(235) Wu, Q. Y.; Zhou, T. H.; Du, Y.; Ye, B.; Wang, W. L.; Hu, H. Y. Characterizing the Molecular Weight Distribution of Dissolved Organic Matter by Measuring

the Contents of Electron-Donating Moieties, UV Absorbance, and Fluorescence Intensity. *Environ. Int.* **2020**, *137* (October 2019). https://doi.org/10.1016/j.envint.2020.105570.

(236) R., A. *Structure and Chemical Composition of Wood: Forest Products Chemistry*; Finland: Finnish Paper Engineers' Association, 2000.

(237) Brezonik, P. L.; Arnold, W. A. Water Chemistry: Fifty Years of Change and Progress. **2012**. https://doi.org/10.1021/es300882y.

(238) Structure and Characteristics of Lignin. In *Lignin Chemistry and Applications*; Huang, J., Fu, S., Gan, L., Eds.; Elsevier, 2019; pp 25–50. https://doi.org/10.1016/B978-0-12-813941-7.00002-3.

(239) Wang, J.; Deng, Y.; Qian, Y.; Qiu, X.; Ren, Y.; Yang, D. Reduction of Lignin Color via One-Step UV Irradiation. *Green Chem.* **2016**, *18* (3), 695–699. https://doi.org/10.1039/c5gc02180d.

(240) Poole, L. B. The Basics of Thiols and Cysteines in Redox Biology and Chemistry. *Free Radic. Biol. Med.* **2015**, *80* (80), 148–157. https://doi.org/10.1016/j.freeradbiomed.2014.11.013.

(241) Schilter, D. Thiol Oxidation: A Slippery Slope. *Nat. Rev. Chem.* **2017**, *1*, 1–2. https://doi.org/10.1038/s41570-016-0013.

(242) Son, S.; Toste, F. D. Non-Oxidative Vanadium-Catalyzed Co Bond Cleavage: Application to Degradation of Lignin Model Compounds. *Angew. Chemie - Int. Ed.* **2010**, *49* (22), 3791–3794. https://doi.org/10.1002/anie.201001293.

(243) Zakzeski, J.; Dbczak, A.; Bruijnincx, P. C. A.; Weckhuysen, B. M. Catalytic Oxidation of Aromatic Oxygenates by the Heterogeneous Catalyst Co-ZIF-9. *Appl. Catal. A Gen.* **2011**, *394* (1–2), 79–85. https://doi.org/10.1016/j.apcata.2010.12.026.

(244) Rahimi, A.; Azarpira, A.; Kim, H.; Ralph, J.; Stahl, S. S. Chemoselective Metal-Free Aerobic Alcohol Oxidation in Lignin. *J. Am. Chem. Soc.* **2013**, *135* (17), 6415–6418. https://doi.org/10.1021/ja401793n.

(245) Ma, R.; Xu, Y.; Zhang, X. Catalytic Oxidation of Biorefinery Lignin to Value-Added Chemicals to Support Sustainable Biofuel Production. *ChemSusChem* **2015**, *8* (1), 24–51. https://doi.org/10.1002/cssc.201402503.

(246) Borges, R. M.; Colby, S. M.; Das, S.; Edison, A. S.; Fiehn, O.; Kind, T.; Lee, J.;

Merrill, A. T.; Merz, K. M.; Metz, T. O.; Nunez, J. R.; Tantillo, D. J.; Wang, L. P.; Wang, S.; Renslow, R. S. Quantum Chemistry Calculations for Metabolomics. *Chem. Rev.* **2021**, *121* (10), 5633–5670. https://doi.org/10.1021/ACS.CHEMREV.0C00901/ASSET/IMAGES/LARGE/CR0C00901_0017.JPEG.

(247) Koch, B. P.; Dittmar, T. From Mass to Structure: An Aromaticity Index for High-Resolution Mass Data of Natural Organic Matter. *Rapid Commun. Mass Spectrom.* **2006**, *20* (5), 926–932. https://doi.org/10.1002/rcm.2386.

(248) Koch, B. P.; Dittmar, T. From Mass to Structure: An Aromaticity Index for High-Resolution Mass Data of Natural Organic Matter. *Rapid Commun. Mass Spectrom.* **2016**, *20* (5), 926–932. https://doi.org/10.1002/rcm.7433 Publi.

(249) Landrum;, G. RDKit. 2010. https://www.rdkit.org/.

(250) Zhang, R.; Yang, Y.; Huang, C. H.; Li, N.; Liu, H.; Zhao, L.; Sun, P. UV/H2O2 and UV/PDS Treatment of Trimethoprim and Sulfamethoxazole in Synthetic Human Urine: Transformation Products and Toxicity. *Environ. Sci. Technol.* **2016**, *50* (5), 2573–2583. https://doi.org/10.1021/acs.est.5b05604.

(251) Huang, Y.; Kong, M.; Coffin, S.; Cochran, K. H.; Westerman, D. C.; Schlenk, D.; Richardson, S. D.; Lei, L.; Dionysiou, D. D. Degradation of Contaminants of Emerging Concern by UV/H2O2 for Water Reuse: Kinetics, Mechanisms, and Cytotoxicity Analysis. *Water Res.* **2020**, *174*. https://doi.org/10.1016/j.watres.2020.115587.

(252) Jaén-Gil, A.; Buttiglieri, G.; Benito, A.; Mir-Tutusaus, J. A.; Gonzalez-Olmos, R.; Caminal, G.; Barceló, D.; Sarrà, M.; Rodriguez-Mozaz, S. Combining Biological Processes with UV/H2O2 for Metoprolol and Metoprolol Acid Removal in Hospital Wastewater. *Chem. Eng. J.* **2021**, *404* (June 2020), 126482. https://doi.org/10.1016/j.cej.2020.126482.

(253) Wang, W.-L.; Xu, Z.-B.; Lee, M.-Y.; Hu, H.-Y.; Huang, N.; Wu, Q.-Y. Potential Risks from UV/H2O2 Oxidation and UV Photocatalysis: A Review of Toxic, Assimilable, and Sensory-Unpleasant Transformation Products. *Water Res.* **2018**, *141*, 109–125. https://doi.org/10.1016/j.watres.2018.05.005.

(254) Wu, C.; Linden, K. G. Degradation and Byproduct Formation of Parathion in Aqueous Solutions by UV and UV/H2O2 Treatment. *Water Res.* **2008**, *42* (19),

4780–4790. https://doi.org/10.1016/j.watres.2008.08.023.

(255) Liu, X.; Liu, Y.; Lu, S.; Wang, Z.; Wang, Y.; Zhang, G.; Guo, X.; Guo, W.; Zhang, T.; Xi, B. Degradation Difference of Ofloxacin and Levofloxacin by UV/H2O2 and UV/PS (Persulfate): Efficiency, Factors and Mechanism. *Chem. Eng. J.* **2020**, *385* (December 2019), 123987. https://doi.org/10.1016/j.cej.2019.123987.

(256) Jaén-Gil, A.; Buttiglieri, G.; Benito, A.; Gonzalez-Olmos, R.; Barceló, D.; Rodríguez-Mozaz, S. Metoprolol and Metoprolol Acid Degradation in UV/H2O2 Treated Wastewaters: An Integrated Screening Approach for the Identification of Hazardous Transformation Products. *J. Hazard. Mater.* **2019**, *380* (January), 120851. https://doi.org/10.1016/j.jhazmat.2019.120851.

(257) Carpinteiro, I.; Rodil, R.; Quintana, J. B.; Cela, R. Reaction of Diazepam and Related Benzodiazepines with Chlorine. Kinetics, Transformation Products and in-Silico Toxicological Assessment. *Water Res.* **2017**, *120*, 280–289. https://doi.org/10.1016/j.watres.2017.04.063.

(258) Abdelraheem, W. H. M.; He, X.; Komy, Z. R.; Ismail, N. M.; Dionysiou, D. D. Revealing the Mechanism, Pathways and Kinetics of UV254nm/H2O2-Based Degradation of Model Active Sunscreen Ingredient PBSA. *Chem. Eng. J.* **2016**, *288*, 824–833. https://doi.org/10.1016/j.cej.2015.12.046.

APPENDIX 1 for Chapter 2

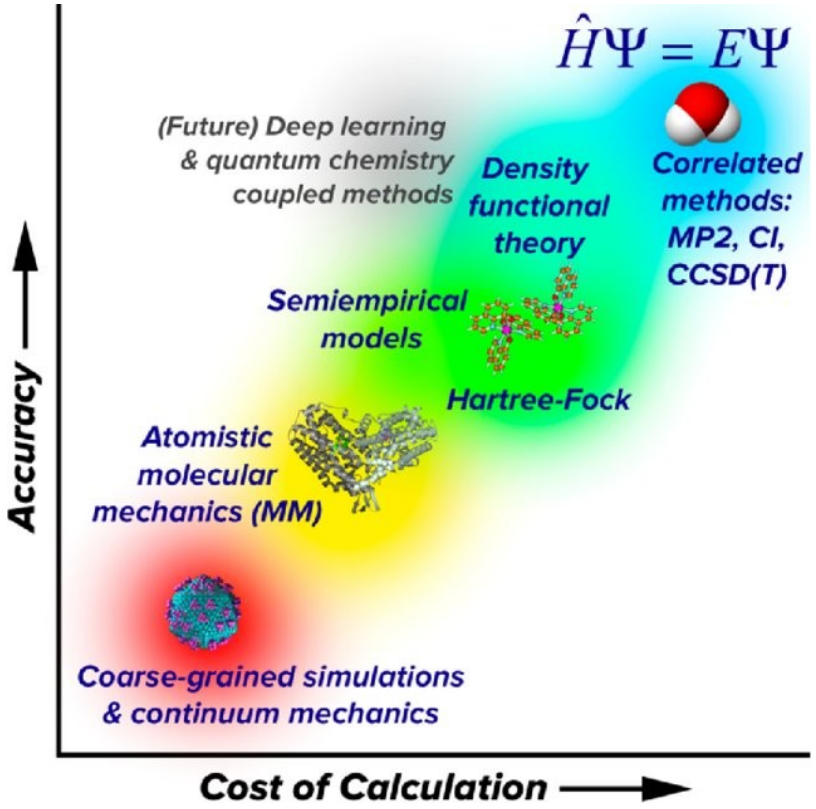

Figure S1 Comparisons between each level of theory in relation with accuracy and cost[246]

Table S1 Fukui index of phenol based on the optimized structure in this research.

Atom number	$f^0(r)$ (×1,000)	% OH• Addition		
		HF		
C-1	0.67	54	ipso	0
C-2	-0.23	0	ortho	99
C-3	0.01	1	meta	0
C-4	-0.11	0	para	1
C-5	0.56	45		
C-6	-1.01	0		
		B3LYP		
C-1	0.55	50	ipso	0
C-2	-0.31	0	ortho	91
C-3	0.09	9	meta	0
C-4	-0.20	0	para	9
C-5	0.46	42		
C-6	-0.78	0		
		M06-2X		
C-1	0.56	42	ipso	0
C-2	-0.40	0	ortho	77
C-3	0.31	23	meta	0
C-4	-0.28	0	para	23
C-5	0.47	35		
C-6	-0.68	0		
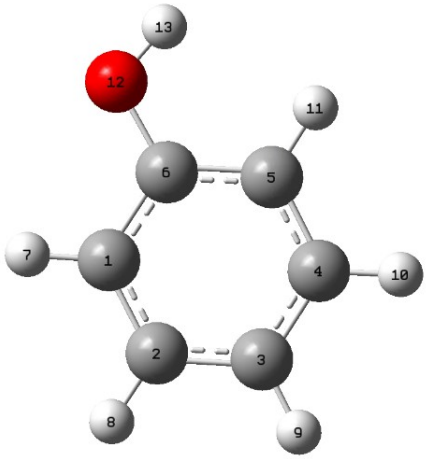				

Table S2 Fukui index of p-DHCH based on the optimized structure in this research.

Atom	$f^{+}(r)$ (×1,000)	% O2 Addition		
		HF		
C-1	-0.55	0	ipso	0
C-2	-1.46	0	ortho	0
C-3	1.65	100	meta	0
C-4	-1.32	0	para	100
C-5	-0.49	0		
C-6	-3.32	0		
		B3LYP		
C-1	-1.94	0	ipso	0
C-2	-0.23	0	ortho	0
C-3	-0.25	0	meta	0
C-4	-0.3	0	para	0
C-5	-1.75	0		
C-6	-0.78	0		
		M06-2X		
C-1	-1.86	0	ipso	39
C-2	2.36	30	ortho	0
C-3	-3.99	0	meta	61
C-4	2.48	31	para	0
C-5	-1.72	0		
C-6	3.13	39		

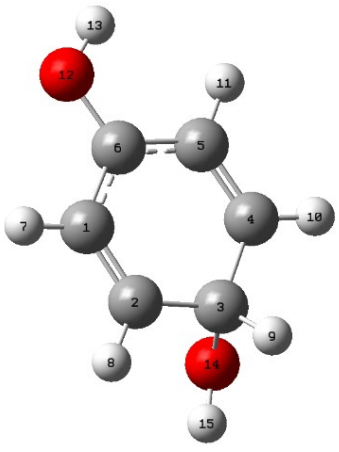

Table S3 Fukui index of p-DHCH.O_2 based on the optimized structure in this research.

Atom	$f^0(r)$ (×1,000)	% HO_2• Abstraction
	HF	
C-1	1.12	18
C-2	0.94	15
C-3	0.96	15
C-4	1.18	19
C-5	1.57	25
C-6	0.4	7
	B3LYP	
C-1	0.76	22
C-2	0.13	4
C-3	1.07	31
C-4	1.16	34
C-5	-0.21	0
C-6	0.36	10
	M06-2X	
C-1	0.93	20
C-2	0.52	11
C-3	1.01	22
C-4	1.18	26
C-5	0.6	13
C-6	0.36	8

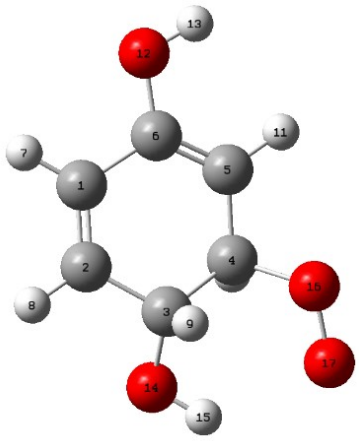

Table S4 Fukui index of o-DHCH based on the optimized structure in this research.

Atom	$f^{+}(r)$ (×1,000)	% O2 Addition		
		HF		
C-1	-2.31	0	ipso	22
C-2	3.05	29	ortho	0
C-3	-3.54	0	meta	78
C-4	5.17	49	para	0
C-5	-3.39	0		
C-6	2.30	22		
		B3LYP		
C-1	-1.91	0	ipso	22
C-2	1.81	30	ortho	0
C-3	-1.96	0	meta	78
C-4	2.85	48	para	0
C-5	-1.85	0		
C-6	1.31	22		
		M06-2X		
C-1	-0.32	0	ipso	26
C-2	3.67	31	ortho	0
C-3	-0.38	0	meta	74
C-4	5.04	43	para	0
C-5	-0.28	0		
C-6	3.13	26		

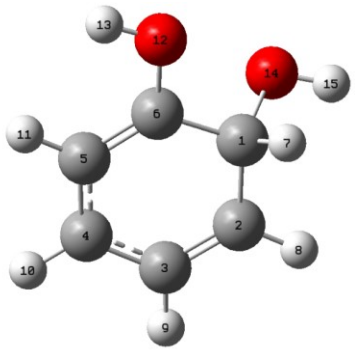

Table S5 Fukui index of o-DHCH.O_2 based on the optimized structure in this research.

Atom	$f^0(r)$ (×1,000)	% HO2• Abstraction
	HF	
C-1	1.03	17
C-2	1.13	18
C-3	1.46	24
C-4	0.60	10
C-5	1.04	17
C-6	0.90	15
	B3LYP	
C-1	1.12	42
C-2	1.07	40
C-3	-0.20	0
C-4	0.41	15
C-5	-0.06	0
C-6	0.07	3
	M06-2X	
C-1	1.02	27
C-2	1.16	31
C-3	0.31	8
C-4	0.55	15
C-5	0.31	8
C-6	0.40	11